REPORT DOCUMENTATION PAGE

Form Approved
OMB No. 0704-0188

1. AGENCY USE ONLY *(Leave blank)*	2. REPORT DATE 22 AUG 97	3. REPORT TYPE AND DATES COVERED

4. TITLE AND SUBTITLE
KALMAN FILTERANALUSIS OF AN ANIMAL HEAD-MOTION ESTIMATION SYSTEM

5. FUNDING NUMBERS

6. AUTHOR(S)
DARRYL LESHUN STEWARD

7. PERFORMING ORGANIZATION NAME(S) AND ADDRESS(ES)
GRADUATE COLLEGE OF THE UNIVERSITY OF ILLINOIS AT URBAN-CHAMPAIGN

8. PERFORMING ORGANIZATION REPORT NUMBER
97-109

9. SPONSORING/MONITORING AGENCY NAME(S) AND ADDRESS(ES)
DEPARTMENT OF THE AIR FORCE
AFIT/CI 2950 P STREET
WRIGHT-PATTERSON AFB OH 45433-7765

10. SPONSORING/MONITORING AGENCY REPORT NUMBER

11. SUPPLEMENTARY NOTES

12a. DISTRIBUTION AVAILABILITY STATEMENT

DISTRIBUTION STATEMENT A
Approved for public release;
Distribution Unlimited

12b. DISTRIBUTION CODE

13. ABSTRACT *(Maximum 200 words)*

14. SUBJECT TERMS

15. NUMBER OF PAGES
46

16. PRICE CODE

17. SECURITY CLASSIFICATION OF REPORT	18. SECURITY CLASSIFICATION OF THIS PAGE	19. SECURITY CLASSIFICATION OF ABSTRACT	20. LIMITATION OF ABSTRACT

ABSTRACT

A climatology of the Cape Canaveral, Florida sea breeze has been established using data from the warm seasons of 1995 and 1996. Data from the Cape Canaveral mesoscale tower network were used to locate the sea breeze, determine its inland penetration, and assess its time of passage. Visible satellite imagery centered over Melbourne, Florida also were used for this purpose. Radiosonde data were used to determine the large-scale flow over the region. A total of 357 days was analyzed. These days were classified as sea-breeze days, non-sea-breeze days, or undetermined. Undetermined days (40) were removed from the final sample, leaving a total of 317 days. River breezes and other local circulations were analyzed and related to the sea breeze, and the presence of convection was related to sea-breeze occurrence and large-scale flow.

An onshore sea breeze was observed on 194 of 317 days (61%) during the warm season. It was likely to form on days with large-scale flow from any direction but northeast. The average time of sea-breeze passage at tower 112 was determined to be 1528 UTC. The sea breeze penetrated the entire Cape Canaveral tower network (30 km) on 81% of the 194 sea-breeze days investigated. Inland penetration was reduced, and passage time was delayed, for offshore flow greater than 4 m s^{-1}. The river breezes that were observed on 116 days tended to occur when the large-scale flow was weak. A trailing convergence line was observed behind the sea-breeze front on 30 days. This line formed on days with weak large-

x

scale forcing. Thunderstorms were observed on 53% of the sea-breeze days, and storms were most likely when the large-scale flow was from the southwest.

Thresholds were established for the onshore and offshore large-scale wind components associated with inland sea-breeze occurrence. Observations indicated an offshore maximum of 12.9 m s^{-1} and an onshore maximum of 6.7 m s^{-1} for the Cape Canaveral area. In general, sea breezes occur over the Cape Canaveral area for onshore flow no greater than 6 m s^{-1} and offshore flow no greater than 10 m s^{-1}. These values are somewhat higher than those derived from previous, numerical studies. Current results indicate that some findings from two-dimensional sea-breeze modeling studies are not applicable to Cape Canaveral's complex land/sea interface.

KALMAN FILTER ANALYSIS OF AN ANIMAL
HEAD-MOTION ESTIMATION SYSTEM

BY

DARRYL LESHUN STEWARD

B.S.E.E., Tuskegee University, 1995

THESIS

Submitted in partial fulfillment of the requirements
for the degree of Master of Science in Electrical Engineering
in the Graduate College of the
University of Illinois at Urbana-Champaign, 1997

Urbana, Illinois

ABSTRACT

Head motion is a parameter that scientists at NASA Ames Research Center are interested in observing during flight experiments. The purpose of determining head motion is to understand the physiological effects of the flight environment upon Rhesus monkeys. Previously, the engineers at Ames Research Center used angular rate sensors to develop head motion velocity (HMV) systems. Although advantages exist for using angular rate sensors to determine head motion, several disadvantages have prompted the engineers at Ames Research Center to investigate new methodology for designing HMV systems. One method employed to avoid the problems associated with using angular rate sensors uses an accelerometer configuration. However, accelerometers are noisy and contain both deterministic and stochastic errors. Hence, this thesis explores using the Kalman filter as a covariance analysis tool to minimize the accelerometer errors and develop an animal head-motion estimation system. Furthermore, the results of several experiments show that an accurate depiction of head motion is obtainable.

DEDICATION

To the memory of the late Sally Leora Robinson. To my family.

ACKNOWLEDGMENTS

First and foremost, I thank God for blessing me with the strength to persevere throughout my pursuit of a graduate education. Next, I thank my advisor, Professor Douglas L. Jones, whose superlative guidance is only superseded by his generosity. Also, I want to thank John W. Hines and the NASA Ames Research Center for supporting this research. Finally, I thank my family, friends, and everyone who has supported my life's endeavors.

TABLE OF CONTENTS

LIST OF TABLES

LIST OF FIGURES

CHAPTER 1

INTRODUCTION

Scientists at NASA Ames Research Center are interested in employing new methodology to process data obtained by the Sensors 2000 biomedical engineering team. These engineers are responsible for developing new sensor technology to measure biomedical parameters during flight experiments. One parameter that they are interested in measuring is the head motion of Rhesus monkeys. The purpose of observing head motion is to allow the principal investigator (PI) the ability to monitor the physiological effects of the flight environment upon the monkey.

The question may be posed, What sensors measure head-motion? especially because countless sensors exist on the market today. No one sensor can completely measure head motion; therefore, head motion velocity (HMV) systems are designed for individual applications. Previously, the engineers at Ames Research Center were using angular rate sensors to measure angular head-motion velocity. An angular rate sensor outputs a voltage that is proportional to the degree of rotation that the sensor experiences. Although advantages exist for using angular rate sensors to design HMV systems, several disadvantages have prompted the Sensors 2000 engineers to employ new methodology to design head-motion systems. To alleviate these problems, one strategy for designing an HMV system is to use an inertial navigation system (INS) design approach. For example, the purpose of an INS system is to determine the position of a vehicle and guide the vehicle from one point to another. An INS is a self-contained unit which utilizes precision gyroscopes and accelerometers to sense all motion of a vehicle [1]. Similarly, an HMV system is also a self-contained unit which is used to process the position and velocity of the head of a monkey at any time. Hence, the use of inertial sensors to gather and process the head motion of a Rhesus monkey is a reasonable assumption. Furthermore, several virtual reality systems use a combination of both angular rate gyros and accelerometers

within head mounted displays (HMDs) to track the head motion of the system user [2]. These HMDs are much too heavy for flight experiments on Rhesus monkeys [2], [3].

The specifications for designing a system to compute the head movement of a Rhesus monkey require special considerations. Because the HMV system will be mounted onto a cap, it is impractical to place heavy hardware onto a little monkey's head. The head-motion system should be as light as possible; however, the sensor circuitry should not compromise the quality of the sensor signals. Another requirement is that the sensor should not create any unwanted disturbances to the monkey during experiments. An advantage of using the angular rate sensor is that it is extremely small; however, it emits a noisy 300 Hz tone that is annoying to the monkey and requires frequent calibration. One method employed to avoid the problems associated with using angular rate sensors is to use an accelerometer configuration. Although the angular rate problems are avoided, accelerometers introduce new errors requiring clever signal processing to remove. These accelerometer errors are caused by sensor misalignment, bias errors, and scale factor errors. Errors normally fall into two categories: deterministic errors and stochastic errors [4]. Deterministic errors are characterized by constant coefficients and may be subtracted out from the system model. An accelerometer bias error falls into this category. Stochastic errors are treated statistically based upon the system's mathematical model. Accelerometer stochastic errors are caused by noise that may be *white* or *colored*, which is accounted for in the plant model of the head-motion system.

This thesis explores designing an HMV system using only accelerometers to process head motion. Several advantages exist for using accelerometers to compute head motion velocity instead of using angular rate sensors or rate gyros. Among the obvious ones are obtaining linear velocity and position. By using these sensors to characterize the head motion of a Rhesus monkey, the direction vector of the head movement may be obtained. The accelerometers used in this HMV circuit cost approximately $30 per sensor; however, some angular rate gyros cost about $2000 per sensor. Clearly, this cost advantage presents an additional incentive to only use accelerometers within the HMV circuitry. If the new system can process the signal output and minimize the accelerometer errors of the system, then the cost advantage is complemented by a reduction in system hardware. Now that

the motivation for using accelerometers is established, the HMV system design procedure consists of designing the system hardware, data acquisition, and postanalysis of the data.

As stated earlier, the approach for designing a head-motion system uses several INS design concepts. Within this methodology is the use of a Kalman filter to determine the system states. The software implements a Kalman filter to obtain the states of the system from the system outputs of the signal circuitry. Although this system post-processes data from a data acquisition board, the discrete-time Kalman filter is intended for real-time implementation in a digital computer. Furthermore, developing a Kalman filter involves using covariance propagation as an error analysis tool. The goal of this thesis is to employ a Kalman filer as a covariance analysis tool to maximize the information obtained from a head-motion system.

The organization of the next four chapters of this thesis is as follows. Chapter 2 develops the notation that is used for the continuous-time and discrete-time models of the Kalman filter. Chapter 3 builds upon the notation developed in Chapter 2 and derives the dynamic equations of linear head motion. Also, Chapter 3 develops a Kalman filter for the head-motion estimation system and discusses the following topics: covariance matrices, the state transition matrix, observations, and Kalman weights. Chapter 4 discusses research methodology used for system design and analysis and is divided into three sections: hardware and software design, test procedures, and results. The last chapter, Chapter 5, discusses conclusions and recommendations.

CHAPTER 2

THE KALMAN FILTER

In this Chapter, we will develop the notation for equations used to implement the Kalman filter. The purpose of a Kalman filter is to estimate the state of a system from measurements that contain random errors. In essence, the Kalman filter consists of a linearized model of the system dynamics which employs statistical estimates of the system error sources. These estimates are then used to compute the time-varying gains of the system to process external measurement information [5].

2.1   The Continuous-time Kalman Filter

We are concerned with estimating the states of a continuous-process head motion from accelerometer measurements. Hence, the continuous-time description of a linear, time-varying state model vector differential equation can be written as

$$\dot{\mathbf{x}}(t) = \mathbf{F}(t)\mathbf{x}(t) + \mathbf{G}(t)\mathbf{w}(t) \tag{2.1}$$

$$\mathbf{z}(t) = \mathbf{H}(t)\mathbf{x}(t) + \mathbf{v}(t) \tag{2.2}$$

where $\mathbf{x}(t_0) = \mathbf{x}_0$, $E[\mathbf{x}_0] = \mu_x$ and $\mathbf{x}(t) \in R^n$ is the state vector, $\mathbf{w}(t) \in R^m$ is the system input vector that consists of white noise, and $\mathbf{z}(t) \in R^r$ is the system output vector. The equation variables are defined as follows:

$\mathbf{x}(t)$ = a state vector of dimension n x 1 representing the error model states

$\mathbf{F}(t)$ = an n x n matrix describing the system and error model dynamics

$\mathbf{G}(t)$ = an n x r matrix which scales the white-noise inputs and sums them with the desired blending of the states x(t)

4

$\mathbf{w}(t)$ = an r x 1 vector of stochastic inputs of a zero-mean white-noise process

$\mathbf{z}(t)$ = an n x 1 vector of the measurement or output vector

$\mathbf{H}(t)$ = an m x n observation matrix relating state $\mathbf{x}$ and measurement $\mathbf{z}$

$\mathbf{v}(t)$ = an m x 1 vector of stochastic observation errors

The solution of the vector differential Equation (2.1) is given by

$$\mathbf{x}(t) = \Phi(t, t_0)x(t_0) + \int_{t_0}^{t} \Phi(t, \tau)G(\tau)w(\tau)d\tau \tag{2.3}$$

where the state-transition matrix $\Phi(t, t_0)$ is a solution of the matrix linear differential equation

$$\dot{\Phi}(t, t_0) = F(t_0)\Phi(t, t_0) \tag{2.4}$$

with the initial conditions

$$\Phi(t, t_0) = I \tag{2.5}$$

where I is the identity matrix, and the state-transition matrix $\Phi(t, t_0)$ can be expressed as

$$\begin{aligned} \Phi(t, t_0) &= [\mathcal{L}^{-1}(sI - F)^{-1}] &\tag{2.6} \\ &= e^{F(t-t_0)} &\tag{2.7} \\ &= I + FT + \frac{(FT)^2}{2!} + \cdots &\tag{2.8} \end{aligned}$$

where $(t - t_0) = \Delta t = T$. Equation (2.2) states that the measurement $\mathbf{z}(t)$ is composed of a linear combination of the state vector with a noise vector $\mathbf{v}(t)$. The observation matrix $\mathbf{H}(t)$ reflects the linear relationship existing between the state and the measurement. We are interested in using noise statistics of the accelerometer to implement the Kalman filter. Assuming that the noise statistics are zero-mean, white, and Gaussian, then the following notations:

$E[\ ]$ = expected value operator

$\mu_x(0)$ = mean of $x(0)$

$$\delta(t) \quad = \quad \text{Dirac delta function}$$

$$\mathbf{Q}(t) \quad = \quad \text{the covariance matrix of the state model uncertainties noise strength}$$

$$\mathbf{R}(t) \quad = \quad \text{the covariance matrix of the measurement noise strength}$$

are used to establish the relations:

$$
\begin{aligned}
E[\mathbf{x}(0)] &= \mu_x(0), \\
E[\mathbf{w}(t)] &= E[\mathbf{v}(t)] = 0, \\
E[\mathbf{w}(t)w^T(\tau)] &= \mathbf{Q}(t)\delta(t-\tau), \\
E[\mathbf{v}(t)\mathbf{v}^T(\tau)] &= \mathbf{R}(t)\delta(t-\tau), \\
E[\mathbf{v}(t)\mathbf{w}^T(\tau)] &= 0,
\end{aligned}
\tag{2.9}
$$

(matrix transpose is denoted by the superscript T).

Now that the notation for the model is established, we can update the best estimate of the state vector x(t) according to a linear combination of the measurements z(t) and the current state estimates $\hat{x}$(t) to minimize the performance index

$$E[\mathbf{x}(t) - \hat{\mathbf{x}}(t)]^T[\mathbf{x}(t) - \hat{\mathbf{x}}(t)] = minimum \tag{2.10}$$

where the solution to minimizing this performance index is the Kalman-Bucy filter [5]. The equation for the optimal state estimator or observer is

$$\dot{\hat{\mathbf{x}}}(t) = \mathbf{F}(t)\hat{\mathbf{x}}(t) + \mathbf{K}(t)[\mathbf{z}(t) - \mathbf{H}(t)\hat{\mathbf{x}}(t)] \tag{2.11}$$

The *Kalman gain* matrix $\mathbf{K}$(t) is a coefficient matrix obtained by solving a *Riccati* differential equation for the error-covariance matrix $\mathbf{P}$(t) where

$$\mathbf{P}(t) = E[\mathbf{x}(t) - \hat{\mathbf{x}}(t)][\mathbf{x}(t) - \hat{\mathbf{x}}(t)]^T \tag{2.12}$$

In Equation (2.12), the difference between the state $\mathbf{x}(t)$ and the measurement $\hat{\mathbf{x}}(t)$ is the error in the estimate.

6

The covariance equation is a Riccati differential equation (RDE). The covariance equation is written as

$$\dot{\mathbf{P}}(t) = \mathbf{F}(t)\mathbf{P}(t) + \mathbf{P}(t)\mathbf{F}^T(t) - \mathbf{P}(t)\mathbf{H}^T(t)\mathbf{R}^{-1}(t)\mathbf{H}(t)\mathbf{P}(t) + \mathbf{G}(t)\mathbf{Q}(t)\mathbf{G}^T(t) \quad (2.13)$$

where $\mathbf{P}(t)$ is a symmetric positive definite matrix which satifies Equation (2.13).

2.2 The Discrete-time Kalman Filter

The HMV data that we receive is continuous; however, we implement the Kalman filter in discrete time [6]. We are interested in processing sampled data from accelerometer measurements to determine optimal estimates of the acceleration, velocity, and position of Rhesus monkey head motion. This section will establish the discrete-time Kalman filter equations that will be used to process the sensor data. Details of the development of these equations may be found in [1], [7], [8].

The following equations implement the discrete-time Kalman filter:

for k=0,1,2,...,

$$\mathbf{x}(k+1) = \Phi(k)\mathbf{x}(k) + \mathbf{w}(k) \quad (2.14)$$

$$\mathbf{z}(k) = \mathbf{H}(k)\mathbf{x}(k) + \mathbf{v}(k) \quad (2.15)$$

where both $\mathbf{w}(k)$ and $\mathbf{v}(k)$ are white Gaussian sequences with zero mean.

State prediction:

$$\hat{\mathbf{x}}(k+1) = \Phi(k)\hat{\mathbf{x}}(k), \quad (2.16)$$

$$\hat{\mathbf{x}}(0|0) = \hat{\mathbf{x}}(0)$$

Observation prediction:

$$\hat{\mathbf{z}}(k+1) = \mathbf{H}\hat{\mathbf{x}}(k+1|k) \quad (2.17)$$

7

Innovations:

$$\mathbf{v}(k+1) = \mathbf{z}(k+1) - \hat{\mathbf{z}}(k+1|k) \tag{2.18}$$

Covariance prediction:

$$\mathbf{P}(k+1|k) = \Phi\mathbf{P}(k)\Phi^T + GQG^T\mathbf{P}(0|0) = \mathbf{P}(0) \tag{2.19}$$

Innovations covariance:

$$\mathbf{S}(k+1) = \mathbf{H}\mathbf{P}(k+1|k)\mathbf{H}^T + \mathbf{R} \tag{2.20}$$

Kalman gain:

$$\mathbf{K}(k+1) = \mathbf{P}(k+1|k)\mathbf{H}^T\mathbf{S}(k+1)^{-1} \tag{2.21}$$

State update:

$$\hat{x}(k+1|k+1) = \hat{x}(k+1|k) + \mathbf{K}(k+1)\mathbf{v}(k+1) \tag{2.22}$$

Covariance update:

$$\mathbf{P}(k+1|k+1) = \mathbf{P}(k+1|k) - \mathbf{K}(k+1)\mathbf{S}(k+1)\mathbf{K}^T(k+1) \tag{2.23}$$

Equations ((2.16)-(2.23)) are used to implement the discrete-time Kalman filter using a computer. The algorithm begins by initially setting the state $\mathbf{X}_0$ and covariance $\mathbf{P}_0$ matrices. Once an incoming measurement $\mathbf{z}(k+1)$ is available, the discrete-time Kalman filter runs a *time-update* step. Before each new accelerometer measurement is processed, the time-update step is resonsible for computing the new accelerations, velocities and positions for the new state matrix $\mathbf{X}(k+1)$ and covariance matrix $\mathbf{P}(k+1)$. The following equations implement the time-update step:

$$
\begin{aligned}
\mathbf{X}^-(k+1|k) &= \Phi\mathbf{X}(k) \\
\mathbf{P}^-(k+1|k) &= \Phi\mathbf{P}(k)\Phi^T + \mathbf{Q}(k)
\end{aligned}
\tag{2.24}
$$

where the superscript $(^-)$ indicates a partial time update.

As in the continuous-time Kalman filter, the prior statistics of w_k and v_k are considered to be zero-mean, white-noise processes. Therefore,

$$
\begin{aligned}
E[\mathbf{x}(0)] &= \mu_x(0), \\
E[\mathbf{w}(k)] &= E\mathbf{v}(k) = 0, \\
E[\mathbf{w}(k)\mathbf{w}^T(j)] &= \mathbf{Q}(k)\delta_{kj}, \\
E[\mathbf{v}(k)\mathbf{v}^T(j)] &= \mathbf{R}(k)\delta_{kj}, \\
E[\mathbf{w}(k)\mathbf{v}^T(j)] &= 0, \forall \; k,j
\end{aligned}
\tag{2.25}
$$

Both the system noise $\mathbf{Q}$ and measurement noise $\mathbf{R}$ covariance matrices may be expressed as follows:

$$
\mathbf{Q}(k) = \begin{bmatrix}
\sigma_1^2 & \sigma_{12}^2 & \cdots & \sigma_{1n}^2 \\
\sigma_{12}^2 & \sigma_2^2 & \cdots & \sigma_{2n}^2 \\
\vdots & \vdots & \ddots & \vdots \\
\sigma_{n1}^2 & \sigma_{n2}^2 & \cdots & \sigma_n^2
\end{bmatrix}
\tag{2.26}
$$

where the cross-correlation system noise terms are denoted by the off-diagonal elements and the diagonal elements are the variances of the noise parameters. The measurement noise matrix $\mathbf{R}$ takes the same form as $\mathbf{Q}$ except that the off-diagonal terms are zero.

$$
E[\mathbf{w}_k\mathbf{w}_j^T] = \begin{cases} \mathbf{Q}_k, & k = j \\ 0, & k \neq j \end{cases}
\tag{2.27}
$$

The noise-strength matrix $\mathbf{Q}(k)$ is given by

$$
E[\mathbf{w}(t_{k+1})\mathbf{w}^T(t_{k+1})] = \mathbf{Q}(t_k) = \int_{t_k}^{t_{k+1}} \Phi(t_{k+1}, \tau)\mathbf{Q}(\tau)\Phi^T(t_{k+1}, \tau)d\tau
\tag{2.28}
$$

Furthermore, the measurement-noise covariance matrix $\mathbf{R}$ is defined as

$$
E[\mathbf{v}_k\mathbf{v}_j^T] = \begin{cases} \mathbf{R}_k, & k = j \\ 0, & k \neq j \end{cases}
\tag{2.29}
$$

which is used to determine the weight that the Kalman filter should place on each of the measurements.

CHAPTER 3

SYSTEM DEVELOPMENT

3.1 System Modeling

The Kalman filter is an optimal linear estimator that minimizes the expected mean-square error in the estimated state variables, given an appropriate system model. This model requires a description of how the state variables change with time in the absence of inputs, and the inaccuracies in both the measurements and the model given that they are characterized by white-noise processes.

Theoretically, a white-noise random process has a power spectral density that is uniform over all frequencies; however, this is not realizable because it implies infinite average power. Nevertheless, many physical systems in nature have a flat power spectrum far higher than the maximum frequency at which a system is responsive [1]. These systems are approximately stationary and Gaussian. Specifically, white noise may be viewed as a limiting form of exponentially correlated noise when the correlation time approaches zero. Experimentation and analysis reveal that using the white-noise concept to design this head-motion system is no exception. As we continue to design the HMV system, we will model any correlated noise by the addition of states to the sytem.

We would like to model each of the accelerometer inputs of the head-motion system as a Gauss-Markov process. For exponentially correlated noise, the autocorrelation function for this zero-mean stationary process is written as

$$R_x(\tau) = \sigma_x^2 e^{-\beta|T|} = \sigma_x^2 e^{\frac{-|T|}{\tau_c}} \tag{3.1}$$

11

and the power spectral density of Equation (3.1) is

$$S_x(\omega) = \frac{2\sigma_x^2 \beta}{\omega^2 + \beta^2} \tag{3.2}$$

where σ_x^2 is the variance of the signal input, $\omega = 2\pi f$ is the frequency, and $\beta = \frac{1}{\tau_c}$. In Equation (3.1) the correlation time is denoted by τ_c. Furthermore, as the accelerometer input correlation time τ_c approaches zero, then

$$R_x(\tau) = \sigma_x^2 \delta(\tau) \tag{3.3}$$

$$S_x(\omega) = 2\sigma^2 \beta. \tag{3.4}$$

We cannot analytically determine the time correlation τ_c of the accelerometers without experimentation. Therefore, we will use these equations to develop a conceptual understanding of the continuous-time system dynamics and investigate determining a correlation coefficient using linear prediction.

3.1.1 Continuous-time model

To process the data obtained from the accelerometers, it is necessary to develop the continuous-time description of the system dynamics. In Chapter 2, the continuous-time description of a linear, time-varying state model can be written as

$$\dot{x}(t) = \mathbf{F}(t)\mathbf{x}(t) + \mathbf{G}(t)\mathbf{w}(t) \tag{3.5}$$

$$\mathbf{z}(t) = \mathbf{H}(t)\mathbf{x}(t) + \mathbf{v}(t) \tag{3.6}$$

Although it is not necessary to fully develop the continuous-time Kalman filter, we are concerned with filtering a continuous-time random process that is driven by what we will assume is white noise.

Therefore, we only need to derive the system-dynamics matrix $\mathbf{F}$ and state-transition matrix Φ, which are valid for both the continuous-time and discrete-time models of the head-motion system. The system-dynamics matrix $\mathbf{F}$ for our system is determined from

the vector **x**

$$\mathbf{x} = \begin{bmatrix} x & \dot{x} & \ddot{x} & y & \dot{y} & \ddot{y} & z & \dot{z} & \ddot{z} \end{bmatrix}^T \tag{3.7}$$

Moreover, **F** can be derived from Equation (3.7) and expressed as

$$\mathbf{F} = \begin{bmatrix} 0 & 1 & 0 & 0 & 0 & 0 & 0 & 0 & 0 \\ 0 & 0 & 1 & 0 & 0 & 0 & 0 & 0 & 0 \\ 0 & 0 & 0 & 0 & 0 & 0 & 0 & 0 & 0 \\ 0 & 0 & 0 & 0 & 1 & 0 & 0 & 0 & 0 \\ 0 & 0 & 0 & 0 & 0 & 1 & 0 & 0 & 0 \\ 0 & 0 & 0 & 0 & 0 & 0 & 0 & 0 & 0 \\ 0 & 0 & 0 & 0 & 0 & 0 & 0 & 1 & 0 \\ 0 & 0 & 0 & 0 & 0 & 0 & 0 & 0 & 1 \\ 0 & 0 & 0 & 0 & 0 & 0 & 0 & 0 & 0 \end{bmatrix} \tag{3.8}$$

Now **F** may be used to determine the state transition matrix. Note that the matrix **F** represents the decoupled dynamics of the head-motion system.

For slowly varying or time-invariant systems, the matrix Φ represents the state-transition matrix. The purpose of the state-transition matrix is to transform a given state at a time t_k to another state at time t_{k+1}. Essentially, this matrix is used to propagate the state covariance matrix **P**. This means that this matrix is used to calculate the state-vector estimate at the present point in time t_k from the previous sample in time t_{k-1}. In our accelerometer problem, we are concerned with propagating the sample t_k to t_{k+1} to adjust the covariance matrix from one sample instant to another. The discrete-time state-transition matrix may be obtained by using **F** to solve the following equation

$$\Phi(t, t_0) = [\mathcal{L}^{-1}(sI - F)^{-1}] \tag{3.9}$$

$$= e^{F(t-t_0)} \tag{3.10}$$

$$= I + FT + \frac{(FT)^2}{2!} + \cdots \tag{3.11}$$

13

where the state-transition matrix $\Phi(t, t_0)$ is used to determine the state of the system given the equation

$$x(t) = \Phi(t, t_0)x(t_0) + \int_{t_0}^{t} \Phi(t, \tau)G(\tau)w(\tau)d\tau \tag{3.12}$$

which yields the state of the system at any time t.

The state-transition matrix of the HMV system is computed using Equation (3.11) so that

$$\Phi_k = \begin{bmatrix} 1 & T & \frac{1}{2}T^2 & 0 & 0 & 0 & 0 & 0 & 0 \\ 0 & 1 & T & 0 & 0 & 0 & 0 & 0 & 0 \\ 0 & 0 & 1 & 0 & 0 & 0 & 0 & 0 & 0 \\ 0 & 0 & 0 & 1 & T & \frac{1}{2}T^2 & 0 & 0 & 0 \\ 0 & 0 & 0 & 0 & 1 & T & 0 & 0 & 0 \\ 0 & 0 & 0 & 0 & 0 & 1 & 0 & 0 & 0 \\ 0 & 0 & 0 & 0 & 0 & 0 & 1 & T & \frac{1}{2}T^2 \\ 0 & 0 & 0 & 0 & 0 & 0 & 0 & 1 & T \\ 0 & 0 & 0 & 0 & 0 & 0 & 0 & 0 & 1 \end{bmatrix} \tag{3.13}$$

where T denotes the sampling time. The state-transition matrix Φ will be used later in the development of the discrete-time model of the system.

Also, notice that the intersection of the first three rows and columns of Φ can be used to write the linear equations of position and velocity, given acceleration for one channel of the system. The decoupled rectilinear equations of motion are

$$x_{\Delta t} = x_0 + Tv_0 + \frac{1}{2}a_{\Delta t}T^2 \tag{3.14}$$

$$v_{\Delta t} = v_0 + a_{\Delta t}T \tag{3.15}$$

where $x(t_0)=x_0$, $v(t_0)=v_0$, and $a_{\Delta t}$ represents acceleration. Now, Equations (3.14) and (3.15) will be used in the next section to develop the discrete-time Kalman filter for the head-motion system.

14

3.1.2   Discrete-time model

As discussed previously, practical implementation of the Kalman filter is done in discrete-time. This is achieved by modeling the dynamics and noise processes of the system into the discrete time form

$$x(k+1|k) = \Phi(k+1|k)x(k) + w(k) \tag{3.16}$$

$$z(k) = H(k)x(k) + v(k) \tag{3.17}$$

where Equations (3.16) and (3.17) represent the state model and the measurement.

Because the continuous-time Equations (3.14) and (3.15) are valid for constant acceleration, the discrete-time model of the system must sample well-above the Nyquist rate to achieve constant acceleration between sample points. The notation for the discrete-time, one-step-ahead state predictor of the head-motion model is denoted as follows:

$$
\begin{aligned}
x_1(k+1) &: \vec{x} \text{ position} \\
x_2(k+1) &: \vec{x} \text{ velocity} \\
x_3(k+1) &: \vec{x} \text{ acceleration} \\
x_4(k+1) &: \vec{y} \text{ position} \\
x_5(k+1) &: \vec{y} \text{ velocity} \\
x_6(k+1) &: \vec{y} \text{ acceleration} \\
x_7(k+1) &: \vec{z} \text{ position} \\
x_8(k+1) &: \vec{z} \text{ velocity} \\
x_9(k+1) &: \vec{z} \text{ acceleration}
\end{aligned}
$$

Given the one-step-ahead state-predictor notation, let us develop the state-space representation for the discrete-time model of the system using the continuous-time Equations (3.14) and (3.15). Here, the discrete-time state equations may be written as

$$x_1(k+1) = x_1(k) + Tx_2(k) + \frac{1}{2}T^2(a_x - \sigma_x)$$

15

$$x_2(k+1) = x_2(k) + T(a_x - \sigma_x)$$

$$x_3(k+1) = (a_x - \sigma_x)$$

$$x_4(k+1) = x_4(k) + Tx_5(k) + \frac{1}{2}T^2(a_y - \sigma_y)$$

$$x_5(k+1) = x_4(k) + T(a_y - \sigma_y)$$

$$x_6(k+1) = (a_y - \sigma_y)$$

$$x_7(k+1) = x_7(k) + Tx_8(k) + \frac{1}{2}T^2(a_z - \sigma_z)$$

$$x_8(k+1) = x_7(k) + T(a_z - \sigma_z)$$

$$x_9(k+1) = (a_z - \sigma_z) \tag{3.18}$$

which represent the states of the system. The three accelerometers are configured orthogonally and output a_x, a_y and a_z which contain errors σ_x, σ_y and σ_z.

The Kalman filter works in a *predict − correct* manner, and modeling the error of the accelerometer measurement as a white-noise process greatly influences the performance of the Kalman filter. This error will be used to compute the input-noise covariance matrix **Q**. In the state Equations (3.18), the values σ_x, σ_y, and σ_z represent the standard deviations of the error of the accelerometer measurements in the $\vec{x}$, $\vec{y}$, and $\vec{z}$ directions, respectively. These input-noise variance statistics are used to minimize the expected mean-square error of the estimated state variables. Also, these noise statistics are used to obtain the value of $\boldsymbol{w}_k$ for Equation (3.16). Furthermore, the matrix representation for the system states may be written as

$$
\begin{bmatrix}
x_1(k+1) \\
x_2(k+1) \\
x_3(k+1) \\
x_4(k+1) \\
x_5(k+1) \\
x_6(k+1) \\
x_7(k+1) \\
x_8(k+1) \\
x_9(k+1)
\end{bmatrix}
=
\begin{bmatrix}
1 & T & \frac{1}{2}T^2 & 0 & 0 & 0 & 0 & 0 & 0 \\
0 & 1 & T & 0 & 0 & 0 & 0 & 0 & 0 \\
0 & 0 & 1 & 0 & 0 & 0 & 0 & 0 & 0 \\
0 & 0 & 0 & 1 & T & \frac{1}{2}T^2 & 0 & 0 & 0 \\
0 & 0 & 0 & 0 & 1 & T & 0 & 0 & 0 \\
0 & 0 & 0 & 0 & 0 & 1 & 0 & 0 & 0 \\
0 & 0 & 0 & 0 & 0 & 0 & 1 & T & \frac{1}{2}T^2 \\
0 & 0 & 0 & 0 & 0 & 0 & 0 & 1 & T \\
0 & 0 & 0 & 0 & 0 & 0 & 0 & 0 & 1
\end{bmatrix}
\begin{bmatrix}
x_1(k) \\
x_2(k) \\
x_3(k) \\
x_4(k) \\
x_5(k) \\
x_6(k) \\
x_7(k) \\
x_8(k) \\
x_9(k)
\end{bmatrix}
+ \mathbf{w}_k \tag{3.19}
$$

where the input-noise statistics w_k will be derived in the following section.

3.2 The Covariance Matrices

3.2.1 The input-noise covariance

The covariance matrix $\mathbf{Q}$ provides a statistical representation of the uncertainty in the current state estimate and the correlation between the individual elements of the states. The HMV system noise covariance matrix is a symmetric matrix that is determined from the following noise-strength equation

$$E[w(t_{k+1})w^T(t_{k+1})] = Q(t_k) = \int_{t_k}^{t_{k+1}} \Phi(t_{k+1},\tau)Q(\tau)\Phi^T(t_{k+1},\tau)d\tau \qquad (3.20)$$

which was discussed in Chapter 2. In practice, it is difficult to determine the input-noise covariance values analytically. However, the approach that was taken for our HMV system was to conduct several controlled experiments and then "tune" the stochastic inputs w_k of the system by estimating the standard deviations of the accelerometers σ_x, σ_y and σ_z.

The performance of the Kalman filter is greatly influenced by modeling the input-white-noise processes using the standard deviation of the input system noise to compute the covariance matrix $\mathbf{Q}$. Therefore, w_k may be expressed as

$$\mathbf{w}_k = \begin{bmatrix} \frac{1}{2}T^2\sigma_x & 0 & 0 \\ T\sigma_x & 0 & 0 \\ \sigma_x & 0 & 0 \\ 0 & \frac{1}{2}\sigma_y^2 & 0 \\ 0 & T\sigma_y & 0 \\ 0 & \sigma_y & 0 \\ 0 & 0 & \frac{1}{2}T^2\sigma_z \\ 0 & 0 & T\sigma_z \\ 0 & 0 & \sigma_z \end{bmatrix} \qquad (3.21)$$

which is used to determine the covariance matrix $\mathbf{Q}$. For the head-motion sytem, we determine the input noise-covariance matrix from the expression

$$\mathbf{Q}(k) = E[\mathbf{w}_k \mathbf{w}_k^T] \tag{3.22}$$

which takes the following form for the HMV system

$$\mathbf{Q} = \begin{bmatrix} \frac{1}{4}T^4\sigma_x^2 & \frac{1}{2}T^3\sigma_x^2 & \frac{1}{2}T^2\sigma_x^2 & 0 & 0 & 0 & 0 & 0 & 0 \\ \frac{1}{2}T^3\sigma_x^2 & T^2\sigma_x^2 & T\sigma_x^2 & 0 & 0 & 0 & 0 & 0 & 0 \\ \frac{1}{2}T^2\sigma_x^2 & T\sigma_x^2 & \sigma_x^2 & 0 & 0 & 0 & 0 & 0 & 0 \\ 0 & 0 & 0 & \frac{1}{4}T^4\sigma_y^2 & \frac{1}{2}T^3\sigma_y^2 & \frac{1}{2}T^2\sigma_y^2 & 0 & 0 & 0 \\ 0 & 0 & 0 & \frac{1}{2}T^3\sigma_y^2 & T^2\sigma_y^2 & T\sigma_y^2 & 0 & 0 & 0 \\ 0 & 0 & 0 & \frac{1}{2}T^2\sigma_y^2 & T\sigma_y^2 & \sigma_y^2 & 0 & 0 & 0 \\ 0 & 0 & 0 & 0 & 0 & 0 & \frac{1}{4}T^4\sigma_z^2 & \frac{1}{2}T^3\sigma_z^2 & \frac{1}{2}T^2\sigma_z^2 \\ 0 & 0 & 0 & 0 & 0 & 0 & \frac{1}{2}T^3\sigma_z^2 & T^2\sigma_z^2 & T\sigma_z^2 \\ 0 & 0 & 0 & 0 & 0 & 0 & \frac{1}{2}T^2\sigma_z^2 & T\sigma_z^2 & \sigma_z^2 \end{bmatrix} \tag{3.23}$$

3.2.2   The measurement-noise covariance

The observation or measurement-noise covariance matrix $\mathbf{R}$ is used to model the standard deviation of the measurement as a white-noise process. Again, it is difficult to analytically determine the values for this process; however, the method used to set the covariances for the HMV system is to "tune" them after calibrating the accelerometers. The HMV system measurement covariance matrix $\mathbf{R}$ is a diagonal matrix which is defined as follows:

$$\mathbf{R}(k) = E[\mathbf{v}_k \mathbf{v}_k^T]. \tag{3.24}$$

Although the HMV system only has one accelerometer input per channel, we model the system as if all of the parameters were measured which allows additional tuning of our system. This concept is discussed further in the next section.

18

3.3   The Observation

The Kalman filter has previously been described to work in a *predict−correct* manner; however, we are limited to have only one sensor observation or measurement. We will illustrate the effect of having only one sensor measurement with an example.

Suppose we have an airplane that contains an accelerometer which measures its vertical acceleration. We want to use a Kalman filter to predict and correct the states of the airplane to obtain its vertical velocity and position. Now let us add an altimeter to the airplane. This altimeter provides additional sensor information regarding the state of the aircraft. The key to this system is that the accelerometer tries to predict the vertical velocity and position of the airplane, and the altimeter reading provides a measurement comparison for the prediction. The difference between the state prediction and measurement is the error. This error is multiplied by the *Kalman gain* to correct the states and update the covariance matrix **P** which is used to process the next sensor measurement.

Now, suppose that we have the same airplane; however, the altimeter is broken. This means that the Kalman filter will have an accelerometer reading, but no comparison for the state predictions. For each state that the Kalman filter cannot measure, it takes a longer time for the covariances of those states to converge to the steady-state value. Moreover, this results in an accumulation of errors that causes the position and velocity to drift over time. Therefore, the *Innovations* step (see Chapter 2) of the Kalman filter will have state predictions that cannot be measured.

Ideally, we would like a measurement for each state of the plant; however, this is not possible. Therefore, we want to trick the Kalman filter into thinking it is receiving actual measurements from every state of the head-motion system. This is done by creating what we will call *virtual measurements*. We will define a *virtual measurement* as an approximation to an actual state measurement for our plant observation by using a linear combination of the measurement from another state. This is feasible, because we can account for the uncertainty in our guess through adjusting the measurement-noise covariance matrix **R**. Hence, these *virtual measurements* are used to add flexibility to the system and provide "tuning."

The Kalman filter uses all of the past and present measurements to provide an estimate of the states of the system. Regardless of the accuracy of the measurement, the HMV system velocity and position estimates are improved by each iteration of the discrete-time update process, and the inputs **w** are a combination of plant dynamics and measurements that are used to form the vector **z**

$$\mathbf{z} = \begin{bmatrix} p & \dot{p} & \ddot{p} & q & \dot{q} & \ddot{q} & r & \dot{r} & \ddot{r} \end{bmatrix}^T \tag{3.25}$$

where

p : *virtual* position measurement in the $\vec{x}$ direction

$\dot{p}$: *virtual* velocity measurement in the $\vec{x}$ direction

$\ddot{p}$: *actual* acceleration measurement in the $\vec{x}$ direction

q : *virtual* position measurement in the $\vec{y}$ direction

$\dot{q}$: *virtual* velocity measurement in $\vec{y}$ direction

$\ddot{q}$: *actual* acceleration measurement in the $\vec{y}$ direction

r : *virtual* position measurement in the $\vec{z}$ direction

$\dot{r}$: *virtual* velocity measurement in $\vec{z}$ direction

$\ddot{r}$: *actual* acceleration measurement in the $\vec{z}$ direction

Furthermore, the values used for the measurement vector **z** may be written as

$$\mathbf{z} = \begin{bmatrix} \frac{1}{2}T^2 a_x & T a_x & a_x & \frac{1}{2}T^2 a_y & T a_y & a_y & \frac{1}{2}T^2 a_z & T a_z & a_z \end{bmatrix}^T \tag{3.26}$$

Now that these modifications to the sytem have been made, the filter weights will be discussed.

3.4   Kalman Weights

The Kalman filter weights or gains **K** affect the *state update* and *covariance update* steps of the Kalman filter. Moreover, the Kalman gain is used to correct what we

observe according to what we claim should have been observed. So for the HMV system, the Kalman gain K is a weight that corrects the observed acceleration, velocity, and position. This gain determines how much we will change the estimate of the state, based on the new observation. One interpretation of this is that if the elements of K are small, then we have considerable confidence in our model, and if they are large, then we are more confident with the observation measurements [6].

Furthermore, the Kalman gain matrix is determined from the relation

$$K = PH^T R^{-1} \qquad (3.27)$$

where P is the covariance prediction, H relates the state to the measurement, and R is the measurement covariance noise matrix. Therefore, we can deduce that K is expressible as

$$K \propto \frac{Q}{R} \qquad (3.28)$$

where Q and R refer to system and observation noises, respectively [9]. Equation (3.28) is interpreted as an increase in filter bandwidth as the Kalman weight K increases. Using the proportionality (3.28), we will tune the system states that use *virtual* measurements. For example, the Kalman gain will be the greatest for the position estimates because they contain the most uncertainty.

CHAPTER 4

RESEARCH METHODOLOGY

4.1 Hardware and Software

The HMV system design procedure consists of developing the system hardware, data acquisition, and postprocessing. The objective of the HMV system hardware design is to reduce the space and weight of the system package without sacrificing sensor information. Another hardware design consideration is the constraint associated with limited flight-environment energy resources. Furthermore, sensor measurements should be immediately available when the system is turned on. The final consideration is that the sensor electronics should provide enough resolution to preserve the low-frequency spectral content that is characteristic of head motion.

4.1.1 The accelerometer

An accelerometer outputs a voltage that is proportional to the amount of force that is acting upon the axis of sensitivity of the sensor. The sensors in the head-motion system are configured mutually orthogonal to detect linear motion in the **XYZ** plane. Considering a neutrally oriented head, the $\vec{x}$ direction extends from the nose outward and is perpendicular to the force of gravity. The $\vec{y}$ direction passes through the ear canal, and the $\vec{z}$ axis parallels the force of gravity. This relationship provides a basis for referencing the information that is received from the states of the system; however, this accelerometer configuration cannot detect the angle of rotation that the head experiences.

The primary consideration for designing the head-motion circuit is in building the system so that the *zero-g bias level* and *output scale factor* of the accelerometers accurately depict the system dynamics. The accelerometers used for this head-motion system
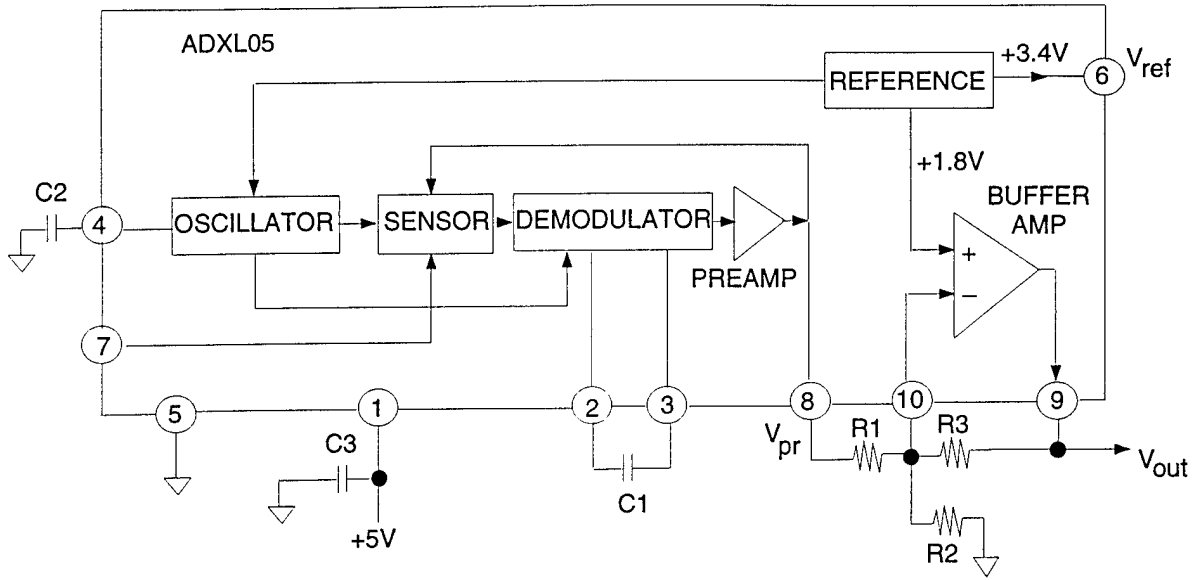
Figure 4.1 Accelerometer Circuit Schematic

are supplied by Analog Devices, and the sensor model type is the ADXL05. The ADXL05 is a 10-pin device that will measure accelerations with full-scale ranges of $\pm 5g$ or less. The noise floor is 500 $\mu g/\sqrt{Hz}$. Each accelerometer circuit uses three external capacitors and shares a +5 volt-regulated power supply. The prototype design for the head-motion system can measure up to $\pm 5g$ accelerations. Also, each circuit uses three resistors to configure the output buffer amplifier, which determines the scale factor of the accelerometer output a_{sf}. The ADXL05 does not need any external signal conditioning to interface to the data acquisition system.

When the ADXL05 is oriented to the earth's gravity (and held in place), the ADXL05 will experience an acceleration of +1 g. This corresponds to a change of approximately + 200 mV at the V_{pr} output pin. Because this is a bipolar device, the output would read negative if the polarity were reversed because of the inverting configuration of the buffer amplifier output V_{out}. Figure 4.1 is the schematic for one accelerometer. Using Figure 4.1, the overall transfer function is

$$V_{out} = \frac{R_3}{R_1}(1.8V - V_{pr}) + \frac{R_3}{R_2}1.8V + 1.8V \qquad (4.1)$$

The nominal values for the components used in Figure 4.1 are given in Table 4.1. By using

23

Table 4.1 Nominal Component Values

Resistor	$K\Omega$	Capacitor	μF
R_1	51	C_1	.022
R_2	270	C_2	.022
R_3	100	C_3	.1

the component values in Table 4.1, the accelerometer output scale factor $a_{sf} = 400mV/g$. Also, the *zero-g bias* is $V_{zg} \approx 2.5V$.

Vectors in three dimensions may be used to analyze the forces that act upon the accelerometer. The ADXL05 is a sensor designed to measure accelerations that result from an applied force. It responds to the component of acceleration on its sensitive x-axis. The sensitive x-axis is defined by a line drawn between the package tab and Pin 5 in the plane of the pin circle. Furthermore, the transverse z-axis and y-axis are used to develop the vector relationship of the forces acting upon the sensor package. The transverse y-axis is the axis perpendicular (90°) to the package axis of sensitivity, and the transverse z-axis is perpendicular to both the package axis and the plane of the pin circle. Figure 4.2 describes a three-dimensional acceleration vector A_{XYZ} acting upon the sensor, where A_X is the component of interest. To determine A_X, it is necessary to find the component of acceleration in the XY plane (A_{XY}) using the cosine law

$$A_{XY} = A_{XYZ}(cos\theta_{XY}) \tag{4.2}$$

$$A_X = A_{XY}(cos\theta_X) \tag{4.3}$$

Therefore, nominal

$$V_{pr} = 200mV/g(A_{XYZ})(cos\theta_{XY})cos\theta_X \tag{4.4}$$

Ideally, the sensor will react to forces along or at angles to its sensitive axis, but will reject signals from its various transverse axes. Moreover, even an ideal sensor will produce output signals if the transverse signals are not exactly 90° from the sensitive X-axis. When an acceleration acts on the sensor from a direction different from the sensitive axis, it will show up at the ADXL05 output at a reduced amplitude. Table 4.2
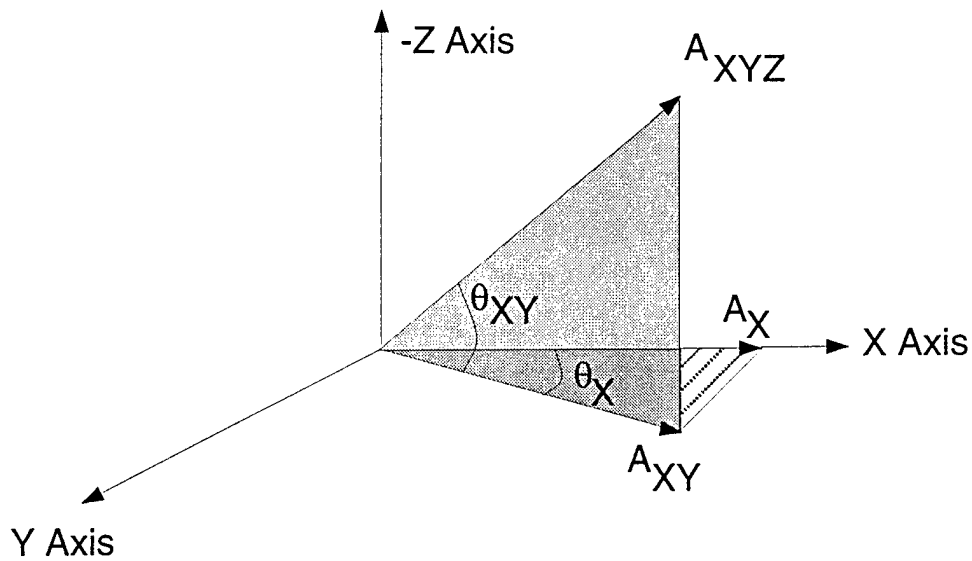
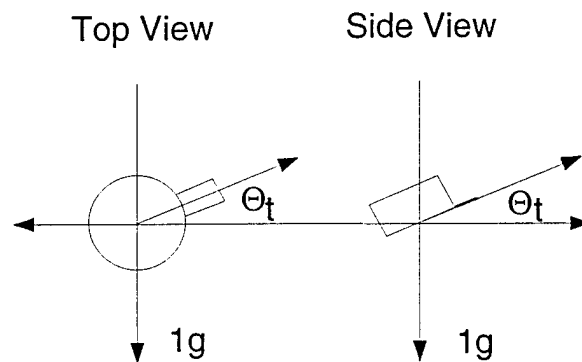**Figure 4.2** Vector Analysis of Forces Acting on Accelerometer

Figure 4.3 Two Possible Tilt Orientations

lists the ideal accelerometer output for forces acting upon various angles of the ADXL05.

Furthermore, another advantage of using the ADXL05 is that it provides tilt measurements. Tilt measurements use the earth's gravity as a constant reference force to determine inclination. This is important to the development of the head-motion system, because it helps determine the error in the accelerometer alignment. The following equation uses the sine function to describe a tilt occurring at an angle θ_t by using gravity as

Table 4.2 Ideal Output for Off-Axis Accelerations

θ_x	% Signal at Output	g Output for $5g$ Acceleration
0°	100	5.000
1°	99.98	4.999
2°	99.94	4.997
3°	99.86	4.993
5°	99.62	4.981
10°	98.48	4.924
30°	86.60	4.330
45°	70.71	3.536
60°	50.00	2.500
80°	17.36	0.868
85°	8.72	0.436
87°	5.25	0.263
88°	3.49	0.175
89°	1.7	0.085
90°	0	0.000

a constant reference force:

$$V_{out} = [a_{sf} \times sin(\theta_t) \times 1g] + V_{zg} \tag{4.5}$$

for accelerometers oriented as in Figure 4.3, where $g = 9.807 m/s^2$, $a_{sf} = 400 mV/g$ is the accelerometer scale factor, and V_{zg} is the *zero-g offset* of the accelerometer.

For a given acceleration signal, and assuming no other changes in the axis or interfering signals, the tilt angle is proportional to the voltage output and is determined using

$$\theta_t = arcsin(1g \times \frac{V_{out} - V_{zg}}{a_{sf}}) \tag{4.6}$$

By using Equation (4.6), each accelerometer tilt error was calculated. It was determined that the largest accelerometer tilt was $\approx 7°$. Uncertainty in the *zero-g offset* and *accelerometer scale factor* may contribute to the tilt error, so we rely upon the convergence properties of the Kalman filter to account for tilt error.

4.1.2 Data acquisition

The data acquistion board, model PC-LPM-16, was developed by National Instrumuents and connects into the parallel port of a personal computer (PC) . The PC-LPM-16 board contains a 12-bit ADC with sixteen analog inputs and a programmable sampling rate up to 50 KHz. This sampling bandwidth well exceeds the Nyquist criteria, which allows high resolution data logging to postprocess the low-frequency, head-motion signals.

4.1.3 Software

The driver software (NI-DAQ) used to control the data acquisition board was also developed by National Instruments. Fortunately, this software was included with the PC-LPM-16 because purchasing application-specific software is extremely expensive, and developing it is time consuming.

The NI-DAQ driver software has a library of functions that may be called from the application programming environment. These functions were used to control the A/D sampling rate and the number of samples per channel collected. The ability to preset the number of samples to data-log is an effective way to conserve PC memory.

4.2 Test Procedures

Before any testing was done, the bias points of the system accelerometers were recorded. This was accomplished by using the constant force of gravity as a reference. The remaining steps in the testing procedure were to conduct the experiments and process the data.

4.2.1 Experimentation

Several experiments were conducted to test the effectiveness of the Kalman filter when applied to the data obtained from the head-motion system. Although no animals were used throughout any of the experiments, each test provided important information regarding the robustness of the Kalman filter to changes within the system inertial dynamics. These experiments were conducted under controlled conditions and fell into two

categories: motionless and dynamic experiments. Motionless experiments were designed to test the convergence of the Kalman filter states and were conducted on a platform. The dynamic experiments were conducted after measuring several trajectories before acquiring data. The dynamics tests were used to analyze the accuracy of the system. Furthermore, the total sampling rate used to collect the data from the three input channels was 200 Hz. Each of the experiments was videotaped to provide additional system analysis information during postprocessing.

4.2.2 Postprocessing

All of the experimental data is postprocessed using MATLAB. MATLAB proved to be an invaluable analysis tool for the development of the head-motion system. Using the system model developed in Chapter 3, MATLAB was used to process the test data by implenting the Kalman filter Equations ((2.16)-(2.23)). The initial postprocessing of the accelerometer data revealed that the head-motion system was extremely noisy. Figure 4.4 is a plot of the motionless accelerometer data and suggests high-frequency noise in the signal. Hence, the corruption of the accelerometer data suggests using a low-pass filter before implementing the Kalman filter. The Parks-McClellan algorithm was used to design a low-pass filter for the noisy accelerometer data. Figure 4.5 is the result of using a low-pass filter of length 51 on Figure 4.4. Further analysis will demonstrate that passing the data through a low-pass filter before implementing a Kalman filter creates several system advantages. The following prefiltering advantages will be shown:

1. An estimate of the accelerometer variances are more readily determined by examining the filtered data.

2. The Kalman filter covariance propagation smoothly converges to the state estimates.

3. A reduction in the mathematical model of the system is achieved, because the state used to determine the acceleration vector is the direct output of the filter.

4. It allows the Kalman filter covariance parameters to focus upon the deterministic errors of the system: tilt, misalignment, zero-g bias, and drifting.
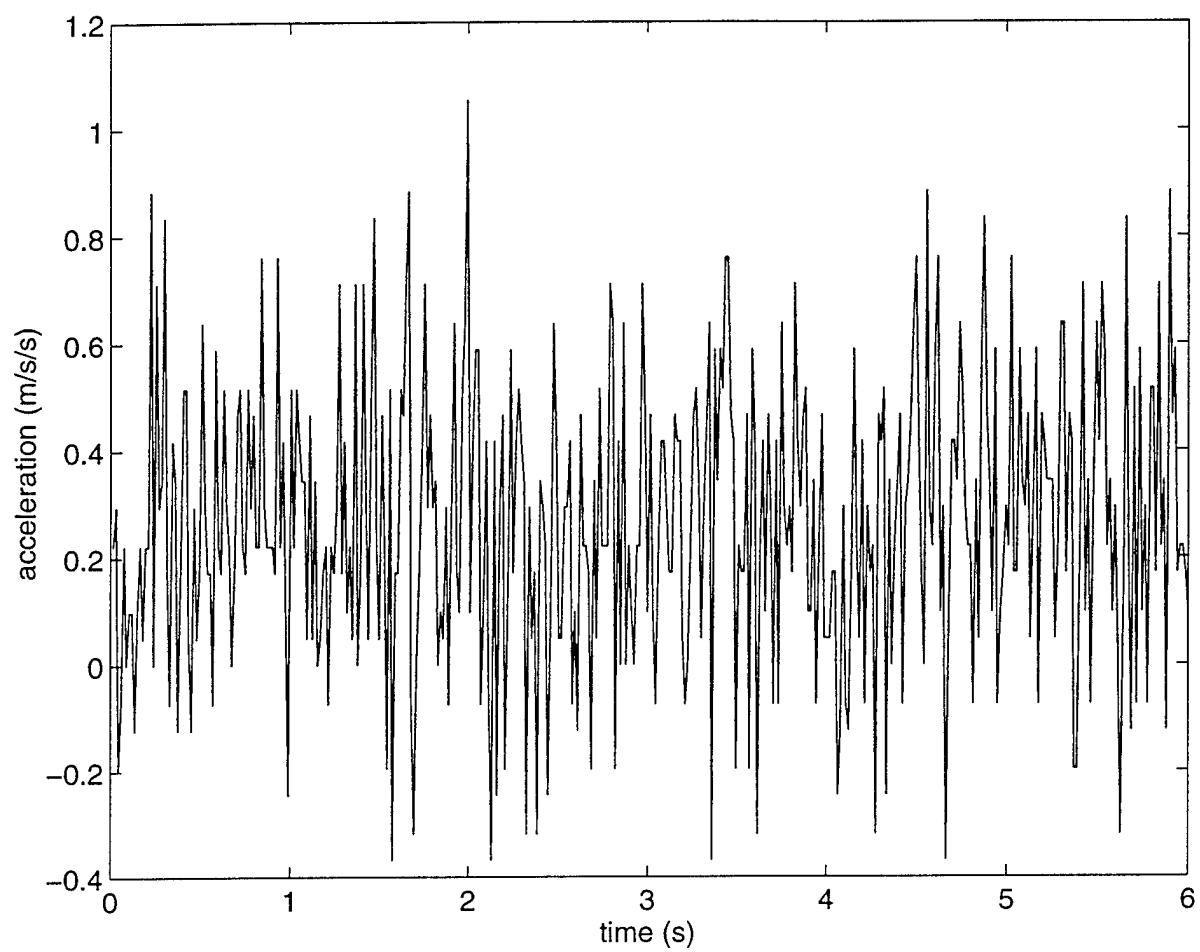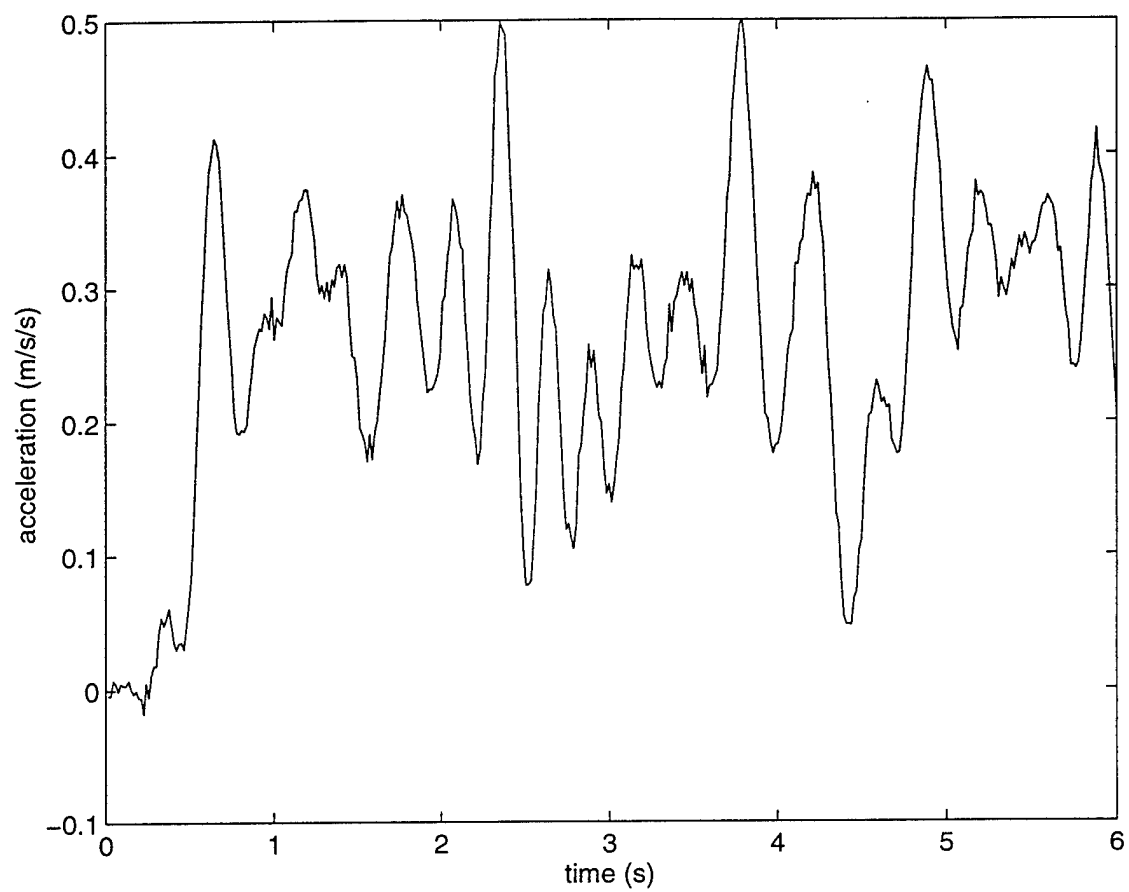
28

Figure 4.4 Unfiltered Y-channel Data

Figure 4.5 Filtered Y-channel Data

4.3 Results

When the accelerometer data are processed with the Kalman filter, the resulting outputs are three state vectors: acceleration, position, and velocity. To evaluate the performance of the Kalman filter upon each test trajectory, we will analyze three different scenarios using the same filter parameters.

- Case 1: The first case will demonstrate the effect of processing a test trajectory after bandlimiting the signal input with a low-pass filter. Although the Kalman filter will not be used in this case, the state-transition matrix Φ will be used to process the system from one state to another.

- Case 2: The second case will examine the effect of processing the same test trajectory data by passing the information directly through the Kalman filter without any prefiltering. This case relies strictly upon the convergence properties of the Kalman filter to obtain the true states of the system.

- Case 3: Essentially, this is a combination of Case 1 and Case 2. The third case analyzes the effect of prefiltering the data before passing the samples through a Kalman filter. It is important to note that a reduction in the system model results because the low-pass filter directly outputs acceleration. Consequently, the Kalman filter uses this filtered acceleration output to determine the velocity and position of the test trajectory.

4.3.1 Test trajectories

Convergence plays a critical role in the development of the Kalman filter [10]. Previously, we noted that the motionless trajectories were designed to test the Kalman filter for convergence. The motionless experiment was conducted on a still platform, and the sensors were free from any external forces. The dynamic experiment consisted of using a hand to generate some data. The hand was constrained to stay within a 10 cm radius and only allowed to move parallel to the force of gravity.

Figure 4.6 represents the X-accelerometer measurement for the raw data (top) and low-pass filter (bottom) for the motionless test.
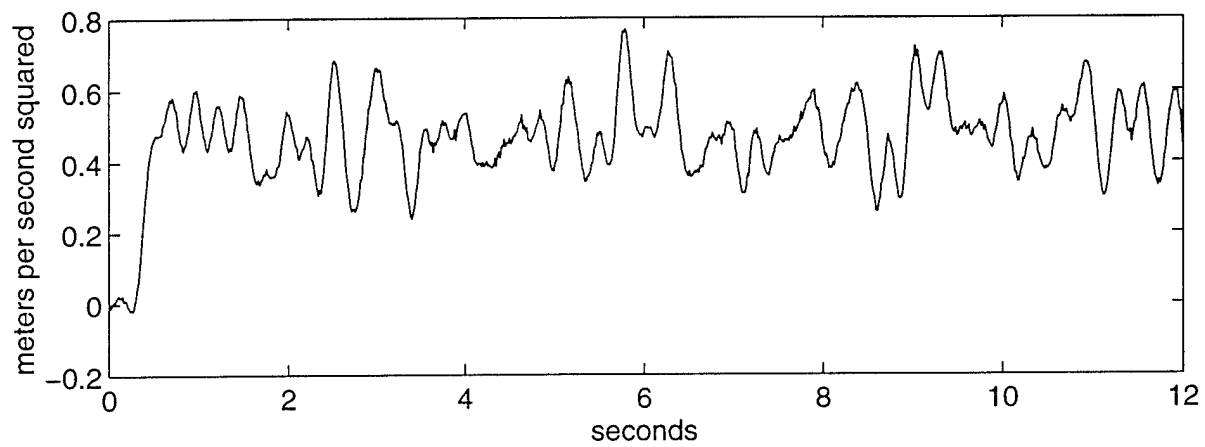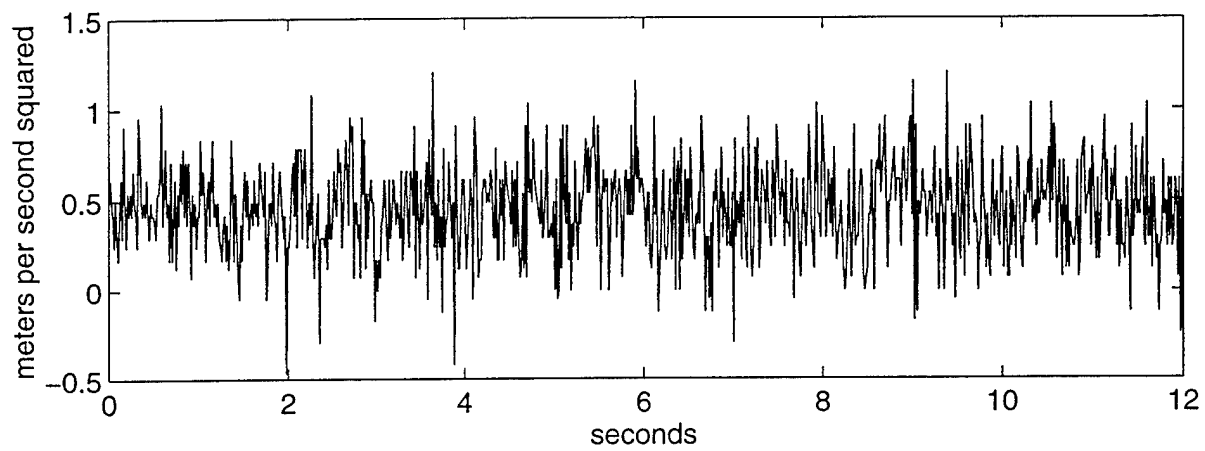
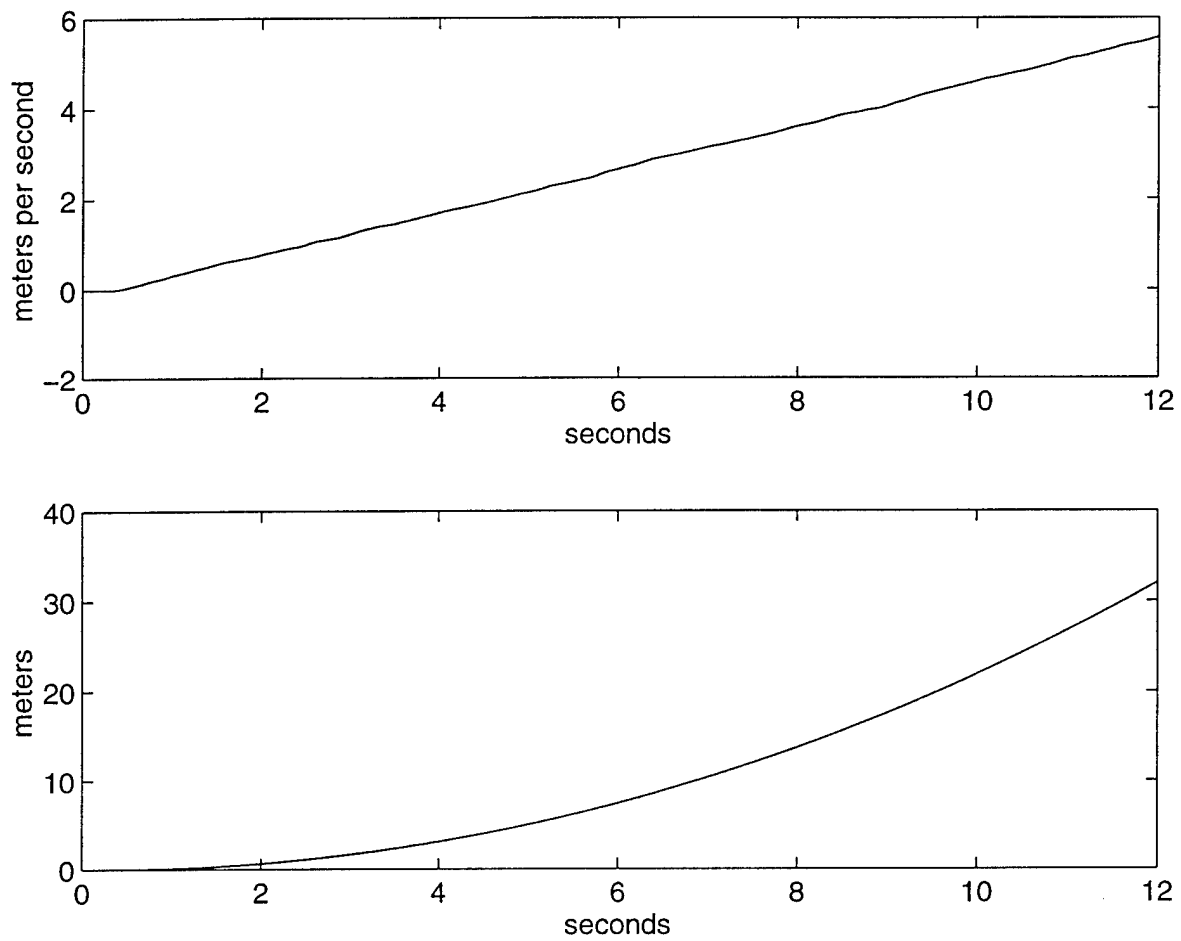**Figure 4.6** Motionless X-accelerometer input

32

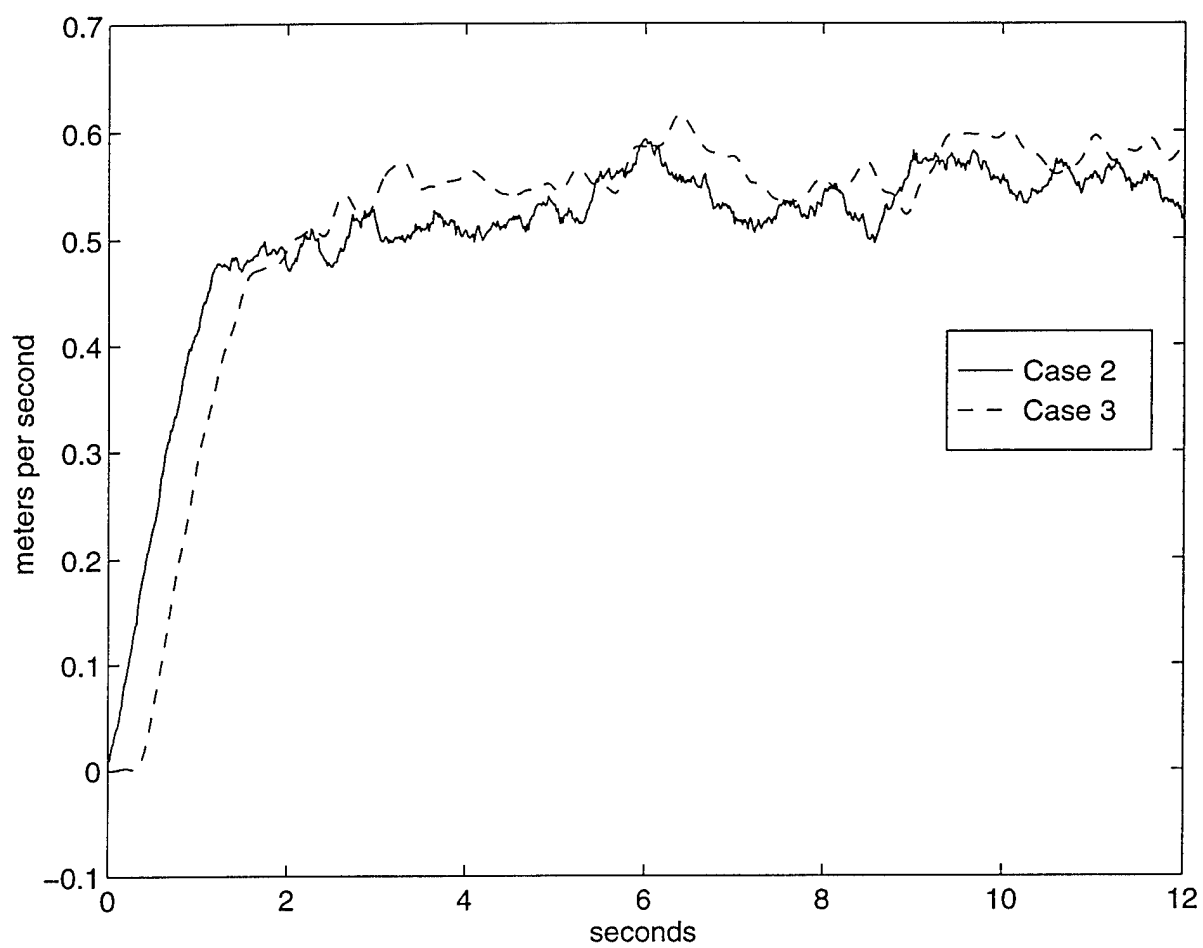**Figure 4.7** X: Unfiltered state-estimate for Case 1
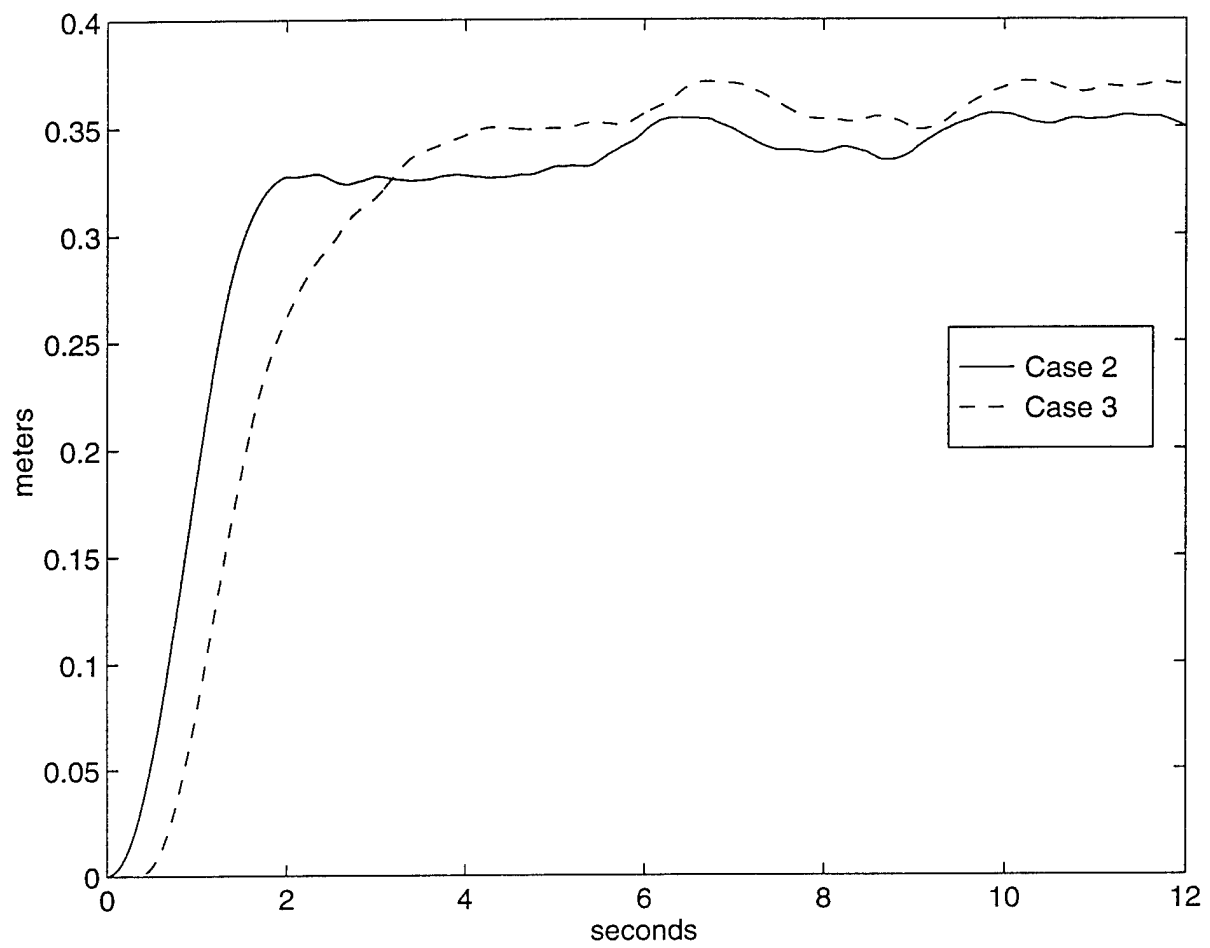
Figure 4.8 X: Velocity estimates

Figure 4.9 X: Positon estimates

4.3.2 System performance

We will examine the convergence properties of this system to rate the system performance. First, the unfiltered velocity and position estimates are displayed in Figure 4.7, Case 1. It is quickly observed that the states of this case diverge. This divergence is expected because the system has no means of compensating for model errors. Next, the velocity and position estimates for Cases 2 and 3 are displayed in Figures 4.8 and 4.9, respectively. The velocity and position estimates both converge. Furthermore, these two cases provide vital information regarding the system dynamics and are worth further analysis. Figure 4.8 shows that the velocity estimate converges when using the Kalman filter; however, the transition is not smooth. Moreover, the position-estimate transition region slope is steep. Recall that Case 3 is the result of both prefiltering and Kalman filtering. This filtering results in a smooth transition region which is shown in Figure 4.9.

The following results are based upon the previously described oscillating hand. Since the majority of motion is in the $\vec{z}$ direction, the Z-channel accelerometer will vary the most. Figure 4.10 represents the Z-accelerometer measurement for the raw data. The unfiltered position estimate for the Z-accelerometer is shown in Figure 4.11. Notice the inaccuracy in the unfiltered position estimate. Next, Figure 4.12 shows the velocity estimates of the oscillating hand. These estimates are approximately the same; however, Case 3 tends to have a smoother transition than Case 2. The position estimates given in Figure 4.13 are approximately identical for Cases 2 and 3. Observe that a time delay results whenever the data are prefiltered.

The next trajectory, Figure 4.14, represents the dynamic Y-accelerometer raw data input. Figure 4.15, shows divergence of the system states. Furthermore, Figure 4.16 depicts the estimated $\vec{y}$ velocity of the oscillating hand. Although the velocity estimation varies, the average velocity is approximately zero. When the oscillating hand tilts, the result is a drift in the velocity estimate. Moreover, when a prefilter and a Kalman Filter are used, the result is a smooth state estimate. Finally, the position estimates shown in Figure 4.17 are similar with the exception of a time delay.
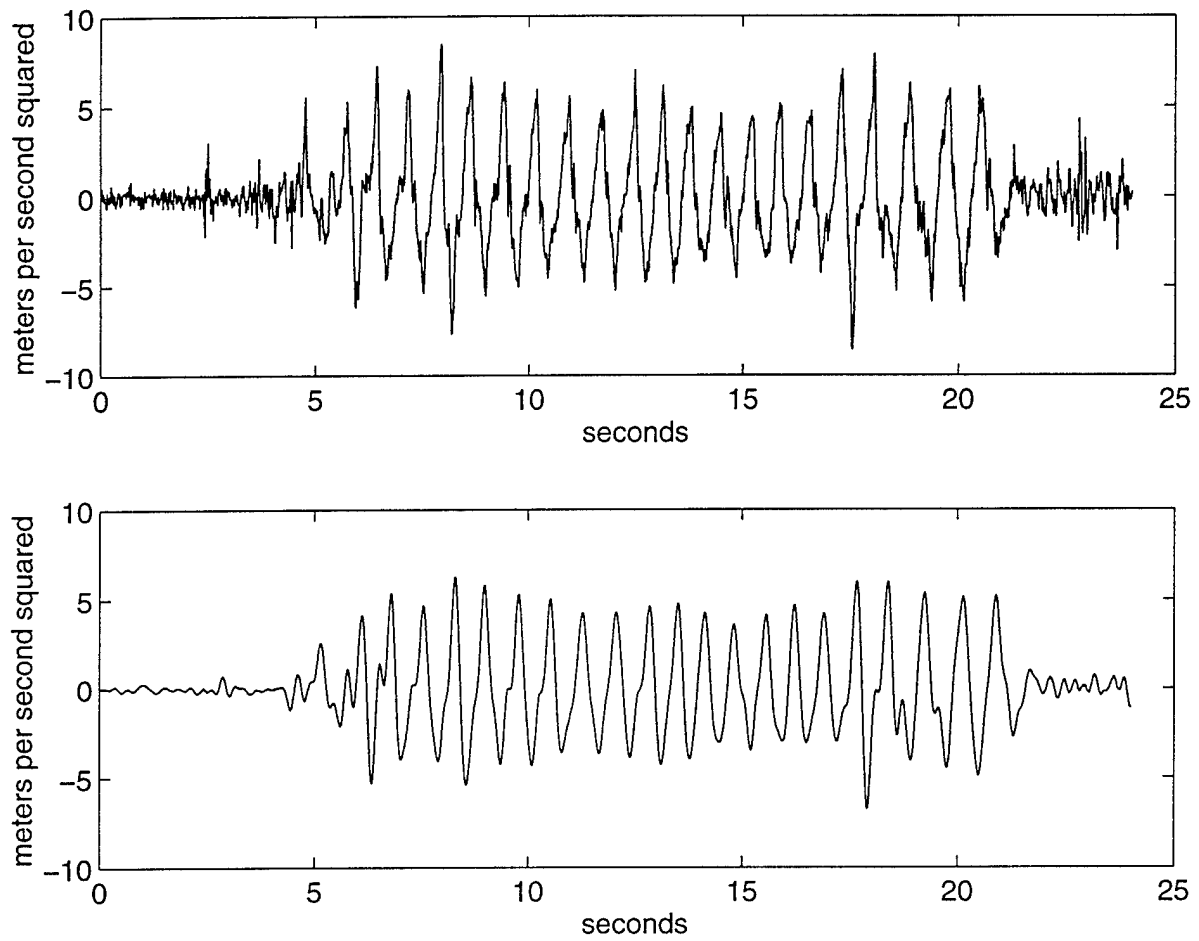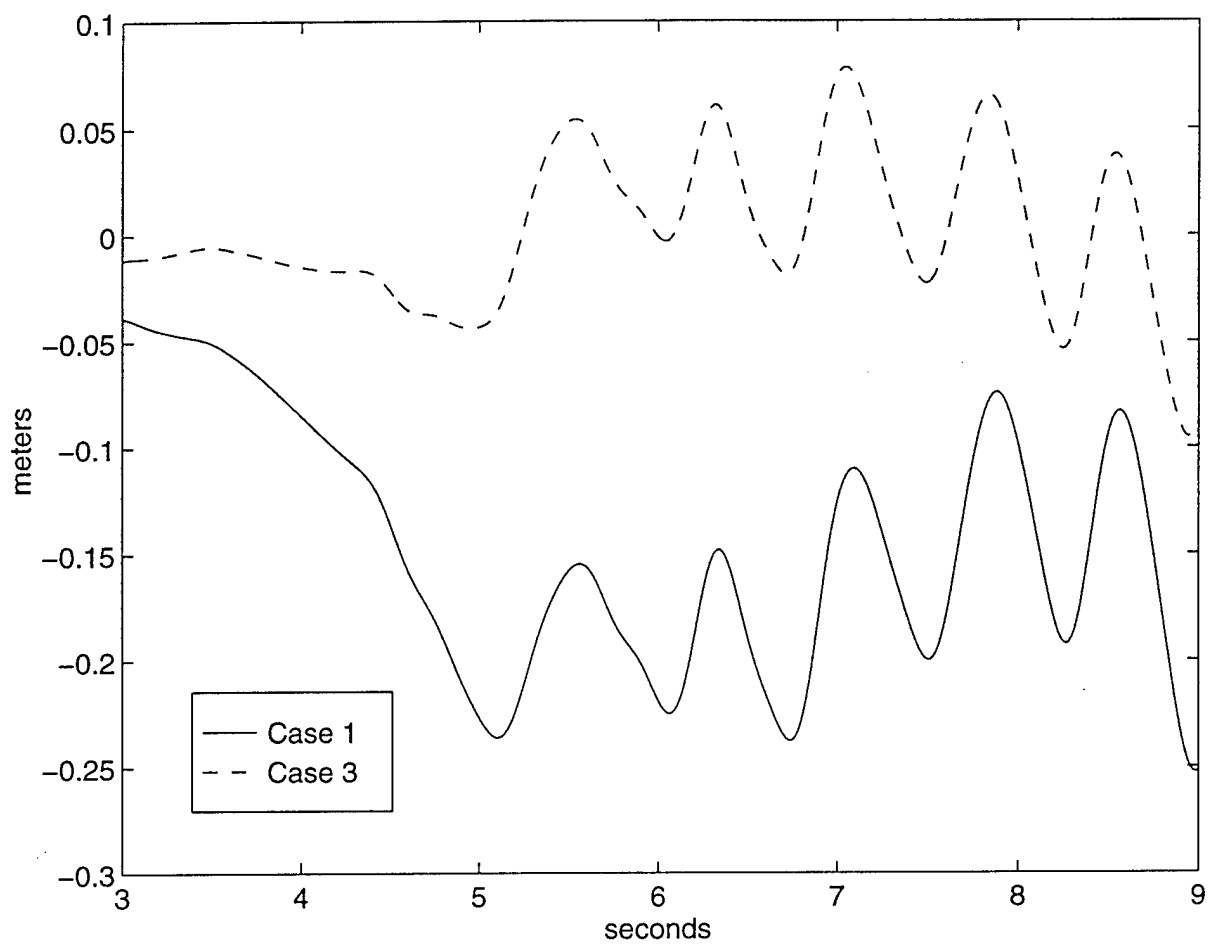
Figure 4.10 Filtered dynamic Z-accelerometer input

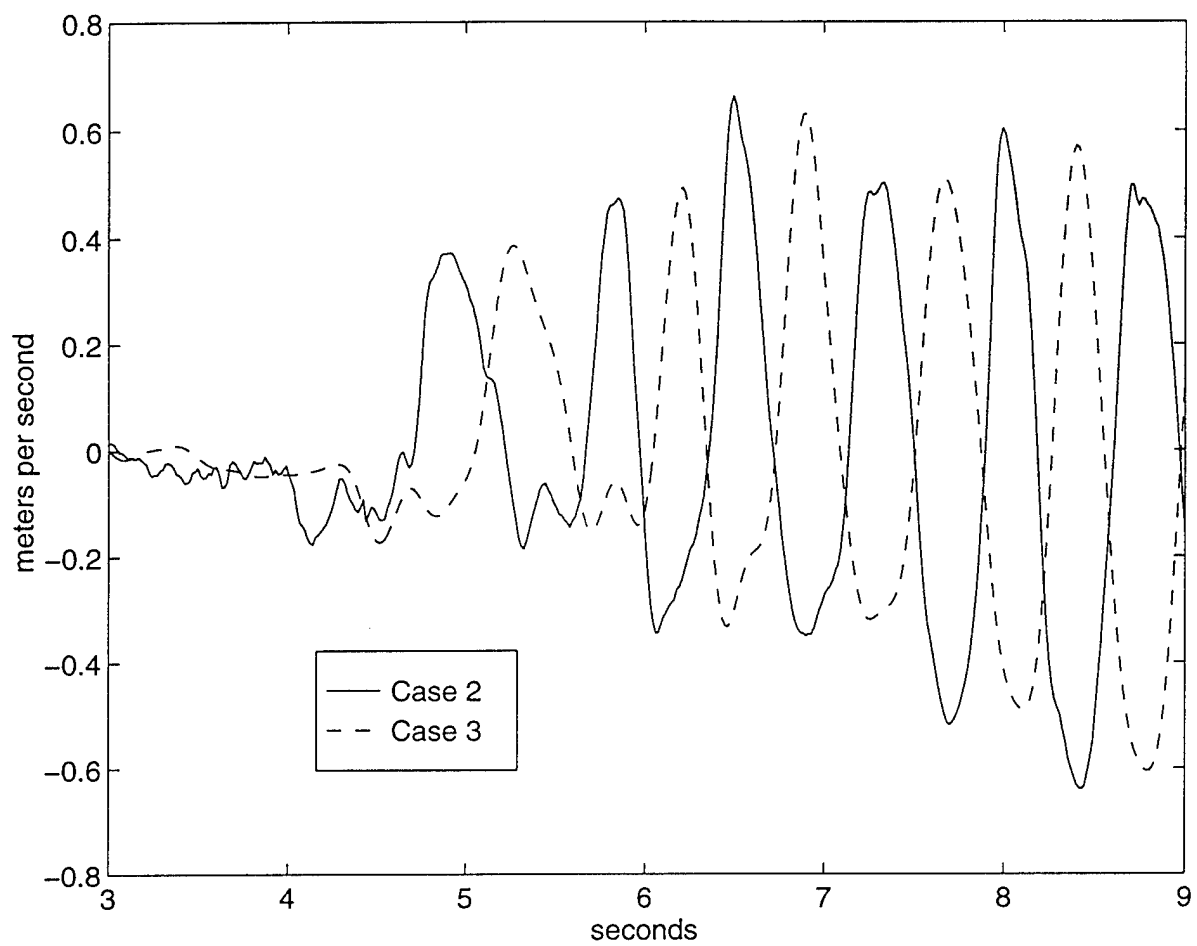**Figure 4.11** Z: Unfiltered position-estimate comparison
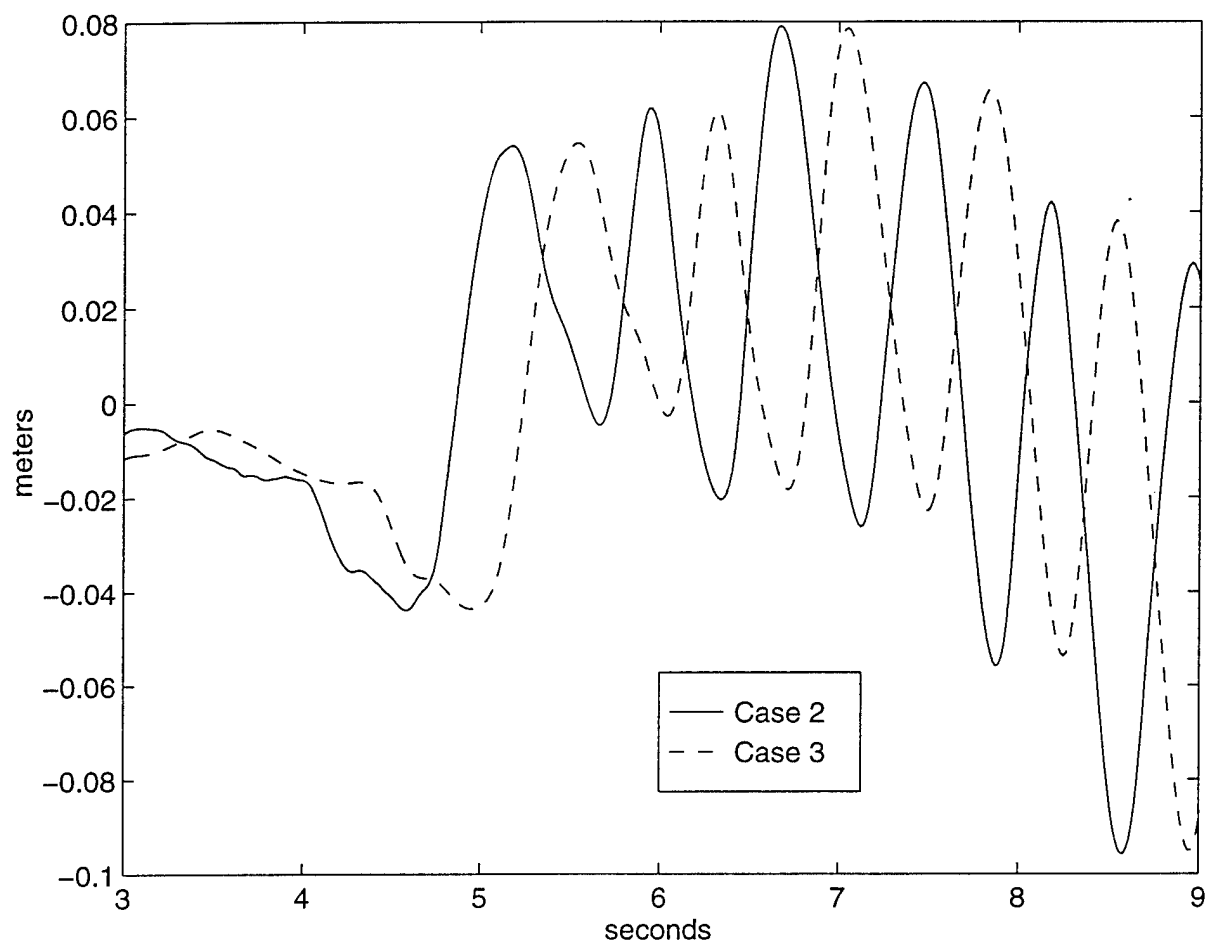
Figure 4.12 Z: Velocity estimates
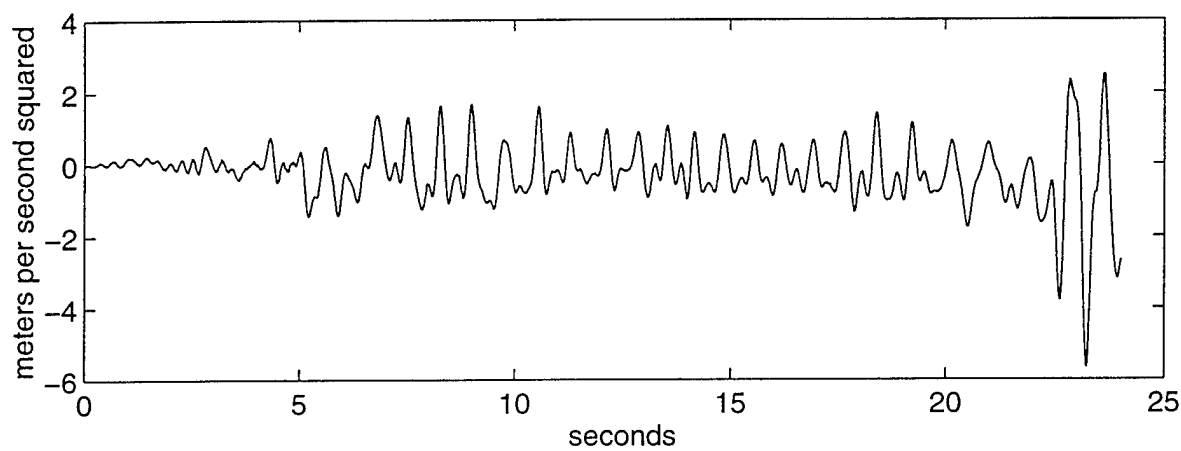
Figure 4.13 Z: Position estimates
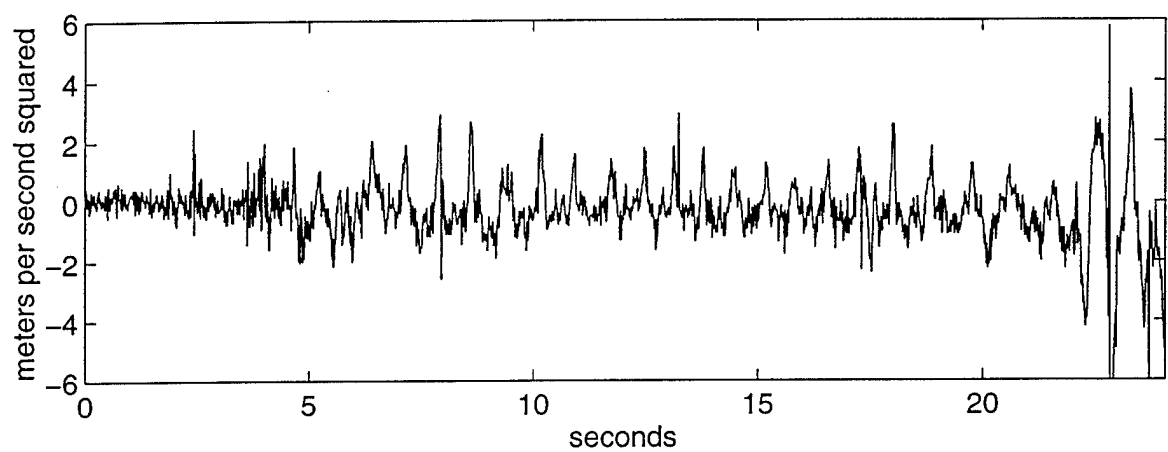
Figure 4.14 Filtered dynamic Y-accelerometer input
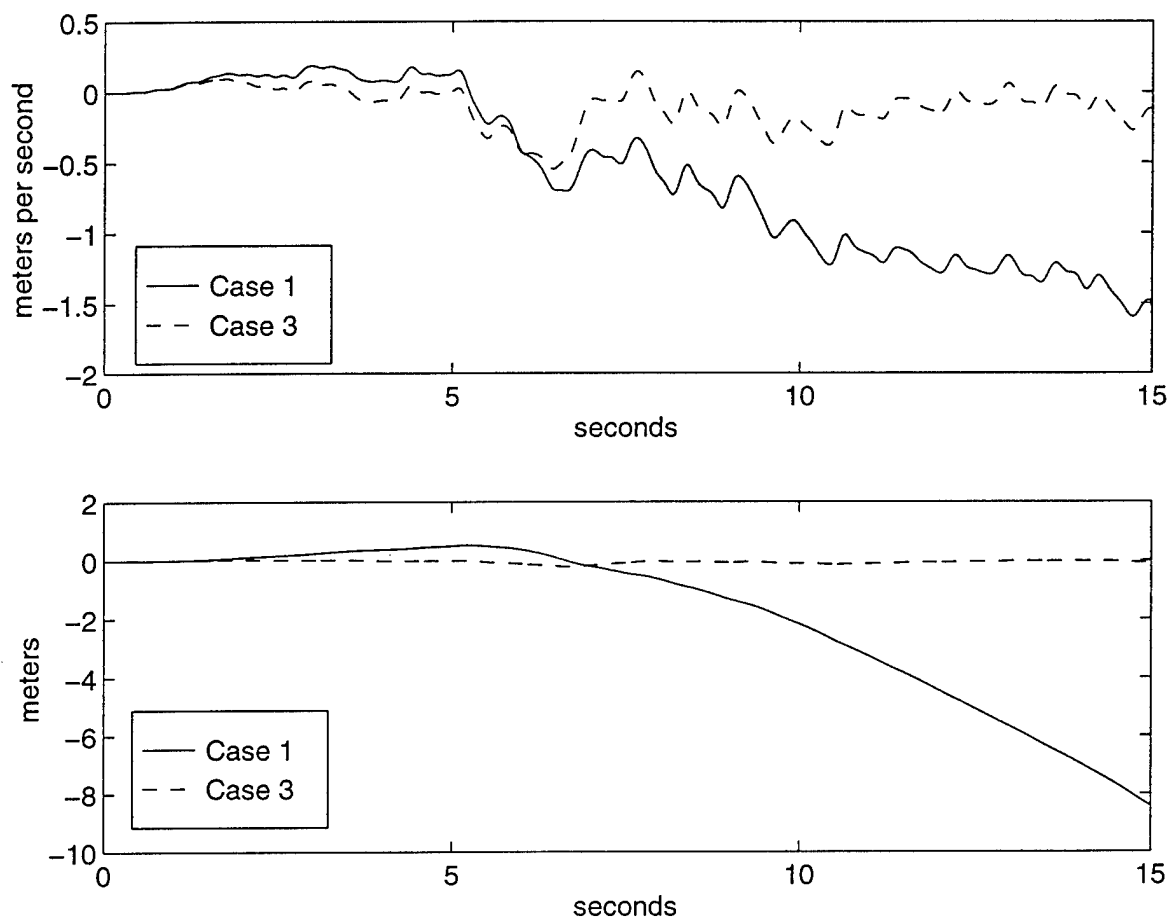
41

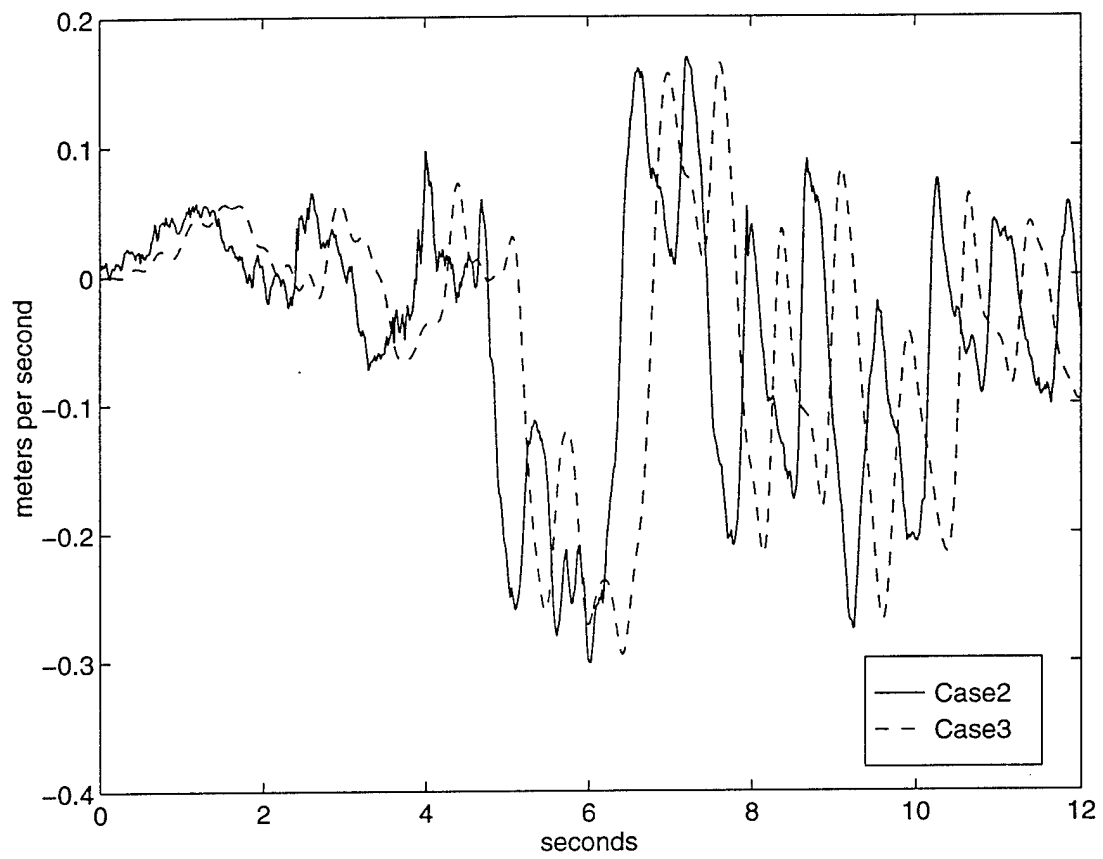**Figure 4.15** Y: Unfiltered state-estimate comparison

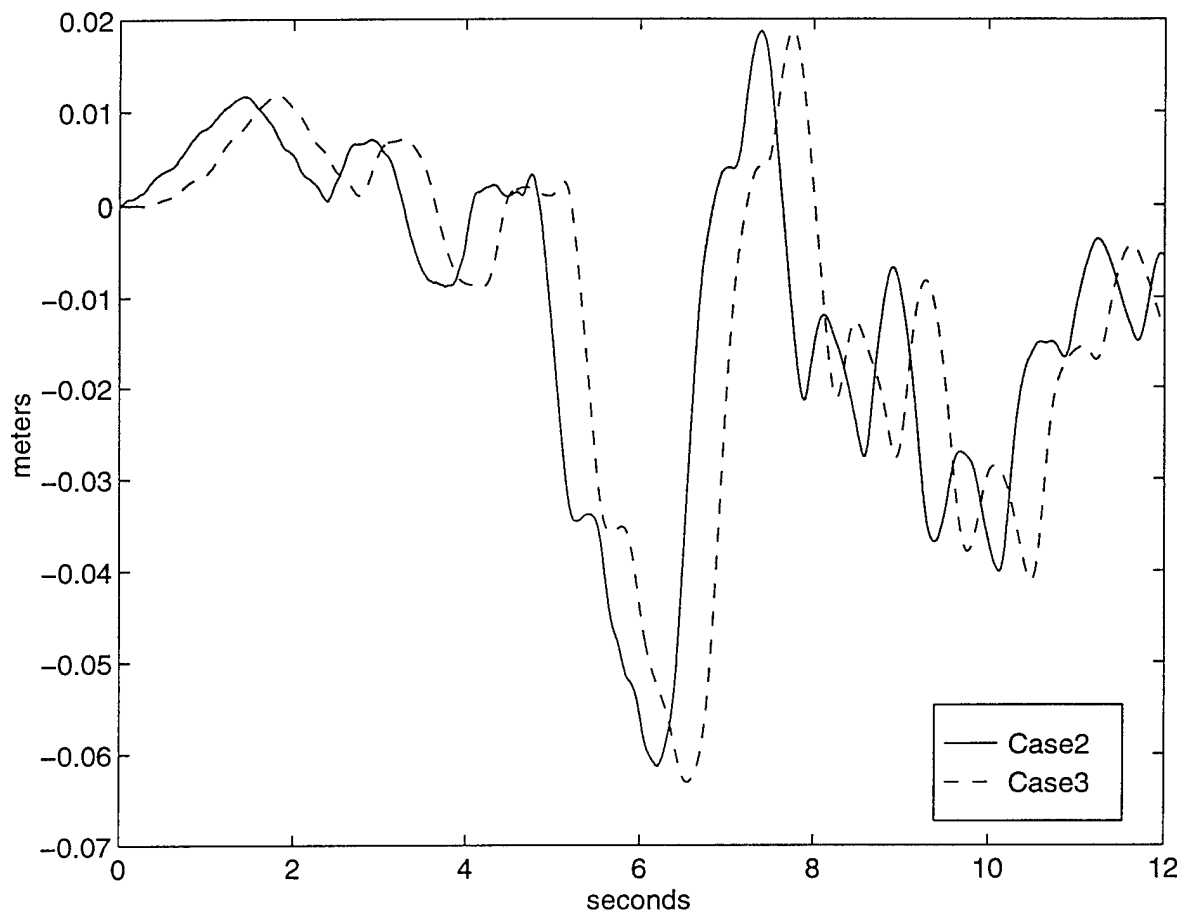**Figure 4.16** Y: Velocity estimates

Figure 4.17 Y: Position estimates

CHAPTER 5

CONCLUSIONS

This thesis has introduced three analysis tools to enhance the quality of information obtained by processing data received from an animal head-motion estimation system. First, we developed a Kalman filter mathematical model for linear head motion. Next, we improved upon this model by introducing *virtual measurements*. Finally, it was shown that preceding the Kalman filter with a low-pass filter significantly improves the state estimates for the head-motion estimation system.

The second analysis tool that we have developed is a *virtual measurement*. These measurement approximations were used in the absence of real state measurements to fit into the mathematical model of the Kalman filter. This technique uses the Kalman filter covariance matrices to constrain the uncertainty within the *virtual measurement*.

The final analysis tool, prefiltering, presents several advantages to improve state estimation for the head-motion system. These prefiltering advantages include the following: a more readily available initialization of the Kalman filter covariance matrices, attenuating high-frequency noise, and smoothing state-estimate transitions. Consequently, future research should analyze the effect of prefiltering sensor data, including the study of the effects of any exponentially correlated noise introduced into the system and how it might affect real-time implementation of this system. Initial analysis suggests that the advantages obtained by prefiltering the data outweigh the disadvantages.

Moreover, further study should develop *self-tuning* algorithms for head-motion estimation. This will improve the robustness of the system and create adaptability to new applications. Future directions for designing head-motion systems should investigate new accelerometer configurations that provide more useful information than an orthogonal configuration.

REFERENCES

[1] G. Siouris, *An Engineering Approach to Optimal Control and Estimation Theory.* New York, NY: John Wiley and Sons, Inc., 1996.

[2] R. Azuma, "Predictive tracking for augmented reality," Ph.D. dissertation, University of North Carolina at Chapel Hill, Chapel Hill, NC, Feb. 1995.

[3] W. Curtis and H. Sowizral, "A note on dynamics of human head motions and on predictive filtering of head-set orientations," *SPIE Proceedings : Telemanipulator and Telepresence Technologies*, vol. 2351, Boston, MA, Oct. 1994, pp. 23-28.

[4] G. Siouris, *Aerospace Avionics Systems: A Modern Synthesis.* San Diego, CA: Academic Press, Inc., 1993.

[5] R. Bucy and P. Joseph, *Filtering for Stochastic Processes with Applications to Guidance*, 2nd ed. New York, NY: Chelsea Publishing Company, 1987.

[6] S. M. Bozic, *Digital and Kalman Filtering.* New York, NY: Halsted Press, 1994.

[7] R. E. Kalman, "A new approach to the linear filtering and prediction problems," *Trans. ASME, D, J. Basis Eng.*, vol. 82, pp. 95-108, March 1961.

[8] S. Mitter, "Filtering and stochastic control: A historical perspective," *IEEE Control Syst. Mag.*, vol. 16, pp. 67-76, June 1996.

[9] J. Candy, *Signal Processing: The Model Based Approach.* New York, NY: McGraw-Hill, 1988.

[10] R. Fitzgerald, "Divergence of the Kalman filter," *IEEE Trans. Autom. Control*, vol. 16, pp. 736-747, Dec. 1971.

REFERENCES

[1] G. Siouris, *An Engineering Approach to Optimal Control and Estimation Theory.* New York, NY: John Wiley and Sons, Inc., 1996.

[2] R. Azuma, "Predictive tracking for augmented reality," Ph.D. dissertation, University of North Carolina at Chapel Hill, Chapel Hill, NC, Feb. 1995.

[3] W. Curtis and H. Sowizral, "A note on dynamics of human head motions and on predictive filtering of head-set orientations," *SPIE Proceedings : Telemanipulator and Telepresence Technologies*, vol. 2351, Boston, MA, Oct. 1994, pp. 23-28.

[4] G. Siouris, *Aerospace Avionics Systems: A Modern Synthesis.* San Diego, CA: Academic Press, Inc., 1993.

[5] R. Bucy and P. Joseph, *Filtering for Stochastic Processes with Applications to Guidance*, 2nd ed. New York, NY: Chelsea Publishing Company, 1987.

[6] S. M. Bozic, *Digital and Kalman Filtering.* New York, NY: Halsted Press, 1994.

[7] R. E. Kalman, "A new approach to the linear filtering and prediction problems," *Trans. ASME, D, J. Basis Eng.*, vol. 82, pp. 95-108, March 1961.

[8] S. Mitter, "Filtering and stochastic control: A historical perspective," *IEEE Control Syst. Mag.*, vol. 16, pp. 67-76, June 1996.

[9] J. Candy, *Signal Processing: The Model Based Approach.* New York, NY: McGraw-Hill, 1988.

[10] R. Fitzgerald, "Divergence of the Kalman filter," *IEEE Trans. Autom. Control*, vol. 16, pp. 736-747, Dec. 1971.